Chapter 6
Measurement Technique

Because meteorological measurements are primarily taken in the near-surface layer, they are carried out in the micrometeorological scale. While some textbooks about meteorological measurements—starting with the classical book by Kleinschmidt (1935)—are available (DeFelice 1998; Brock and Richardson 2001; Emeis 2010; Hebra 2010; Harrison 2015), it can be challenging to find detailed information about micrometeorological measurement and data processing techniques. For this reason, a special chapter is dedicated to micrometeorological measurements. Unlike other books with extensive descriptions of meteorological instrumentation, only general principles of the micrometeorological measurement techniques are described. Of special importance are techniques for the optimal adaptation of the sensors to the surrounding environment—the turbulent atmosphere. The quality assurance of observations is another focal point.
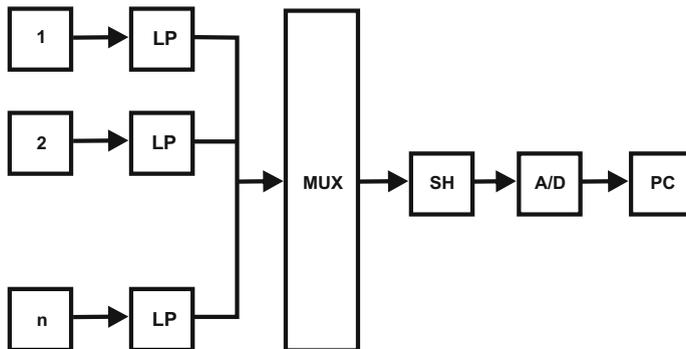
6.1 Data Collection

Digital data collection systems have recently replaced analogue systems. Due to their inertia, analogue systems often required only simple filter functions; however, for digital recording systems these functions are not simple. This is a topic for the users but not the producers, who developed their loggers mostly for universal applications. For the development of micrometeorological measurement systems, the following basic considerations must be made.

6.1.1 Principles of Digital Data Collection

Modern data collection systems use data loggers that collect quasi-parallel signals and create a serial digital signal for transmission to a computer or a storage unit.

Thus, each signal is sampled regularly in time, which is the sampling frequency. This sampling frequency must be adapted very precisely to the frequency of the measured signal. For sensors with a high time resolution (e.g. sonic anemometers), the sensor itself is no longer a low pass filter (LP). An additional low-pass filtering (see Sect. 6.1.2) must be provided so that at the input of the logger no frequencies occur that are greater than half of the sampling frequency. Often, the low pass filtering is done with the software of the sensor. Thus, the signal of the sensor is sampled with a frequency, which is much greater than necessary. The signal is then averaged over several samplings (over sampling). This low pass filtering has the benefit that often-present noise of 60 (50) Hz from the power supply has no influence on the input signal of the logger, which could otherwise affect spectral analyses (aliasing).

With a multiplexer (MUX), the signals of the individual sensors are successively sampled. Then, the sampling process starts again from the beginning. For turbulence measurements, covariances are often calculated between different logger channels, and the logger must be programmed in such a way that signals for covariance calculations are sampled at neighbouring channels. Grounding unused logger channels prevents noise from influencing the system. The logger submits the measured signals one after the other over a sample and hold circuit (SH) to an analogue-to-digital converter (A/D), whose configuration influences the accuracy of the system. While often in the past only 11 or 12 bits were resolved, recent converters have mostly 16-bit resolution of the signal. For the configuration of the logging system, attention must be paid so that there is enough time available for converting the signals, which must be tuned with the sampling frequency. The high sampling frequencies required for turbulence measurements are close to the limits of the loggers. A basic circuit of a data sampling system is shown in Fig. 6.1.

Fig. 6.1 Basic circuit of a data sampling system with 1 to n signals, low passes (LP), multiplexer (MUX), sample and hold circuit (SH), analogue-digital converter (A/D), all integrated in a modern logger and a data collection computer (PC) or storage medium

The analogue-to-digital converter is responsible for the discretization of the signal amplitude. The specification must be dependent on the noise level, S, between the signal level and the mean noise level, where the logarithmic measure $S_{dB} = 10 \lg S$ is used. Using

$$S_{dB} = 1.76 + 6.02n, \tag{6.1}$$

with the bit resolution, n, of the A/D converter, the minimal distance to the noise level in decibel (dB, see Supplement 6.1) or the separation from the noise level (Profos and Pfeifer 1997) can be determined.

Supplement 6.1 Specification of amplification and damping in decibel

The amplification or damping of a measurement system is given by a logarithmic proportion (Bentley 2005):

$$X_{dB} = 20 \lg \frac{X_2}{X_1} \tag{S6.1}$$

This ratio is applied for amplifiers with the output voltage X_2 and the input voltage X_1 respectively for the damping of filters. The measurement unit is the logarithmic proportion expressed in decibel (dB). For power (e.g. product of voltage and current) one uses:

$$P_{dB} = 10 \lg \frac{P_2}{P_1} \tag{S6.2}$$

This measure is also used to express the noise level. If the signal differs from the noise level by factor 10^6, then the distance to the noise level is 60 dB.

6.1.2 Signal Sampling

Micrometeorological data often must be sampled with a high time resolution, e.g. for eddy covariance measurements, the sampling frequency is about 20 Hz. Even for standard meteorological data the sampling rate is 1 Hz. The sampling rate determines the discretization in time. Accordingly, the measured signal must be on the A/D converter a long enough time so that the signal level can be adjusted and digitized. The time difference between two samples depends on the conversion time and the number of measurement channels. The sampling of a periodic function g (t) must be done in such a way that the measured data can be reconstructed for the given sampling time Δt. The necessary number of samples is given by the sampling theorem (Schrüfer et al. 2014):

According to the sampling theorem a function $g(t)$ with sampling values $g(x_i)$ in a time period Δt can be exactly reconstructed, if their Fourier spectra S (k) for $k > \pi/\Delta t$ disappears. The sampling period Δt must be chosen so that $\Delta t < 1/(2 f_g)$ where f_g is the highest resolvable frequency.

This means that periodic oscillations must be sampled more than two times per period or the sampling frequency must be double of the measurement frequency (Bentley 2005; Schrüfer et al. 2014). The frequency

$$f_N = \frac{1}{2\Delta t} > f_g \tag{6.2}$$

is called Nyquist frequency. Therefore, the highest appearing frequency, f_g, must be limited by low pass filtering, and is equal to the frequency where a damping of 3 dB occurs. If higher frequencies nevertheless occur, e.g. by noise of the power frequency, the so-called aliasing effect will appear (Bentley 2005):

The aliasing effect is a false reconstruction of a continuous function g (t) made from discreetly-sampled values $g(x_i)$ with a time resolution of Δt, resulting in higher frequencies appearing as lower ones.

In Fig. 6.2, it is shown that for accurate sampling the function (f1) can be correctly reconstructed while functions with higher frequencies (f2) cannot be reconstructed. In spectra of signals with aliasing the energy of lower frequencies increases ($<f_g$). The increase is equal to the energy of the not-included frequencies above f_g. Therefore, no energy loss happens, but the frequencies are not correctly reconstructed. For frequencies that are not related to the measurement process (electrical power frequency), false measurements occur. If the power frequency cannot filtered, then the sampling frequency should be chosen in such a way that the power frequencies compensate each other, e.g. for 60 Hz power frequency a sampling frequency of 30 Hz and for 50 Hz one of 25 Hz (Kaimal and Finnigan 1994).

Meteorological measurement systems are already low pass filters (see Sect. 4.2.3.3). Due to the finite extension of the sensors, the only turbulence elements that can be measured are larger than or equal to the measurement path d. Furthermore, due to the turbulence spectrum the filter frequency depends on the wind velocity and the measurement height. As a simple approximation for the upper frequency limit with 10% damping and a height of 5–10 m, one can use according to Mitsuta (1966):

$$f_{g10\%} = \frac{u}{d} \tag{6.3}$$
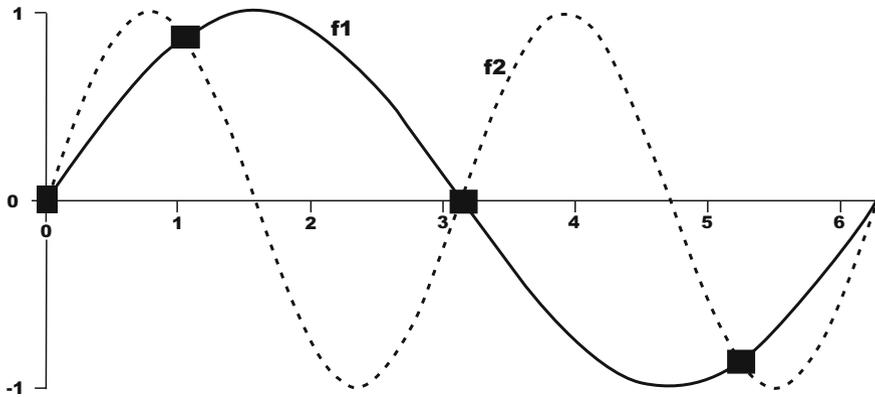
Fig. 6.2 Sampling of periodic signals: f1 is correctly represented in contrast to f2

Another simple approximation with the wind velocity and the measurement height (Kaimal and Finnigan 1994) is:

$$f_g > 8\frac{\overline{u}}{z} \tag{6.4}$$

The length of a measured time series depends on the lowest frequency of the turbulence spectrum to be constructed. Attention must be paid so that for an acceptable accuracy of the standard deviations and covariances a minimum of samples is necessary. According to Haugen (1978), this is at least 1000, and is illustrated for different quantities in Fig. 6.3. In the case of statistical independence, the error is approximately $N^{-1/2}$ (N: umber of samples). Because the independence of time series is generally uncertain a higher error must be assumed (Bartels 1935; Taubenheim 1969).

For spectral analysis, the length of the necessary time series is determined by the accuracy of the low frequency part of the spectrum. Assuming an error of 10%, the length, T, must be chosen so that either it is the 10 times the longest period to reconstruct or the lower frequency limit given by $f_{gl} = 10/T$ (Taubenheim 1969). This measurement length is generally significantly longer than those for the error calculation for standard deviations and covariances.

6.1.3 Transfer Function

In addition to inadequate sampling of the measurement signal an inadequate resolution in time and space of the sensor itself can also cause measurement errors. A transfer function of a measurement system describes the time delay between the output signal and the input signal (phase shift) and the damping of the amplitude.
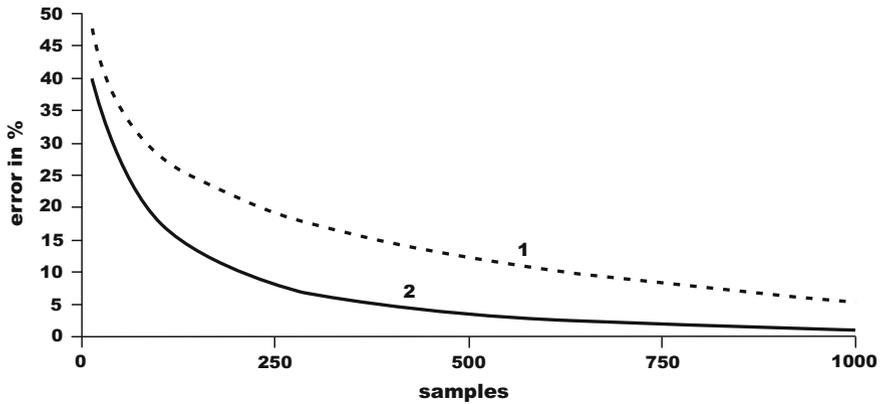
Fig. 6.3 Error in the measurements of (*1*) the friction velocity or the sensible heat flux; (*2*) error in the standard deviation of the vertical wind component as functions of the number of samples. Processed on the basis of the results of Haugen (1978)

A transfer function can be defined in the space of the complex Laplace operator $s = \delta + i\omega$, with δ as a damping parameter (see Supplement 6.2):

$$T(s) = \frac{L\{X_s(T)\}}{L\{X_i(T)\}} \tag{6.5}$$

The determination of the Laplace transform of the sensor output signal, X_s, from the Laplace transform of the input signal, X_i, is given by:

$$X_s(s) = X_i(s)T(s) \tag{6.6}$$

This description is very simple for many practical applications. For example, the product of the single functions can determine the transfer function of a measurement system. For a turbulence measurement system, the transfer function can be determined as the product of the transfer functions of the response in time, of the averaging by the sensor in space, and by the averaging in space of sensors that are used for eddy-covariance measurements at a certain distance (Eq. 4.49).

The error of a standard deviation or of a flux is given by the ratio of the spectrum multiplied with the transfer function to the undamped spectrum:

$$\frac{\Delta F}{F} = 1 - \frac{\int\limits_0^\infty T_{x(y)}(f)S_{x(y)}(f)df}{\int\limits_0^\infty S_{x(y)}(f)df} \tag{6.7}$$
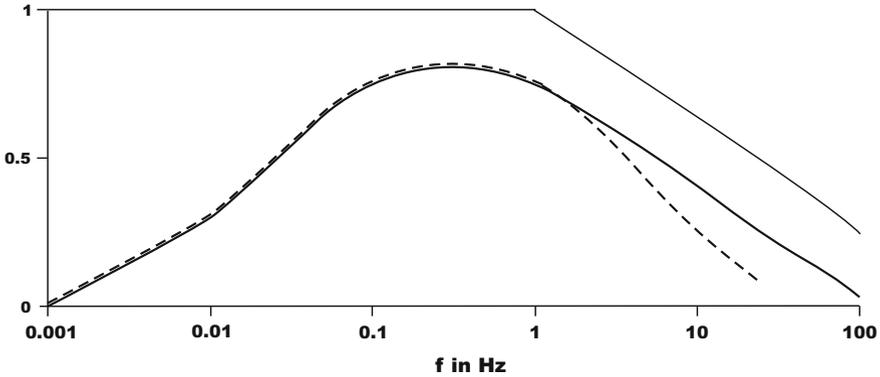
Fig. 6.4 Schematic graph of the transfer function T (*thin line*) and the turbulence spectra S (*thick line*) with the resulting spectra $T\,S$ (*dotted line*)

Figure 6.4 shows schematically that the turbulence spectrum is reduced if the transfer function is less than one. Because in most of the cases the damping starts in the inertial subrange, the correction of turbulence measurements for well-known turbulence spectra is relatively simple. The spectrum in the inertial subrange is extrapolated or corrected relative to the modelled spectra, e.g. Moore (1986).

Supplement 6.2 Laplace transformation

In contrast to the Fourier transformation (see Supplement 2.3), which is a function of circular frequency, the Laplace transform transformation of an aperiodic signal, which disappears for $t < 0$, is a function of a complex operator $s = \delta + i\omega$ (Bentley 2005). The Laplace transformed L is defined as:

$$X(s) = L\{X(t)\} = \int_{0}^{\infty} X(t)\, e^{-st} dt \tag{S6.3}$$

For the backward transformation is:

$$X(t) = L^{-1}\{X(s)\} = \frac{1}{2\pi i} \int_{s=\delta-i\omega}^{\delta+i\omega} X(s)\, e^{st} ds \tag{S6.4}$$

A benefit of the Laplace transformation is that extensive tables and software for the determination of the transformation are available (Doetsch 1985; Graf 2004).

6.1.4   Inertia of a Measurement System

A special case of a transfer function is the sharp change of the signal from $X = X_0$ for $t \leq t_0$ to $X = X_\infty$ for $t > t_0$. A first-order measurement system, e.g. temperature measurements, can be described by the differential equation (Profos and Pfeifer 1997; Brock and Richardson 2001):

$$X_s(t) = X_i(t) + \tau \frac{dX_i}{dt} \qquad (6.8)$$

The dependency of the input X_i and output X_s signals can be presented with the time constant τ. To have an indicator number, which is dependent only on the sensor and not on the size of the quantity for different meteorological systems, different indicator numbers are used. For second order measurement systems (wind vane) see DeFelice (1998) or Brock and Richardson (2001).

6.1.4.1   Time Constant

For a first order measurement systems and assuming $X_0 = 0$ the differential equation Eq. (6.8) has an exponential solution

$$X(t) = X_\infty \left(1 - e^{-\frac{t}{\tau}} \right), \qquad (6.9)$$

where X_∞ is the final value after complete adjustment to the surrounding conditions and τ is the time constant which is a measure of the inertia of the measurement system:

> The time constant of a measurement system is the time required for the measurement system to reach 63% of its final or equilibrium value. The value of 63% is equal to $(1 - 1/e)$.

To determine the real final value due to a sharp change of the input signal, it is necessary to measure significantly longer than the time constant. This value depends on the required accuracy, and should be at least five times the time constant. The response of the measurement signal after a sharp change is schematically shown in Fig. 6.5.

6.1.4.2   Distance Constant

Anemometers have a wind-speed dependent time constant, i.e. time constants are not representative specifications for anemometers. Instead, a distance constant, can
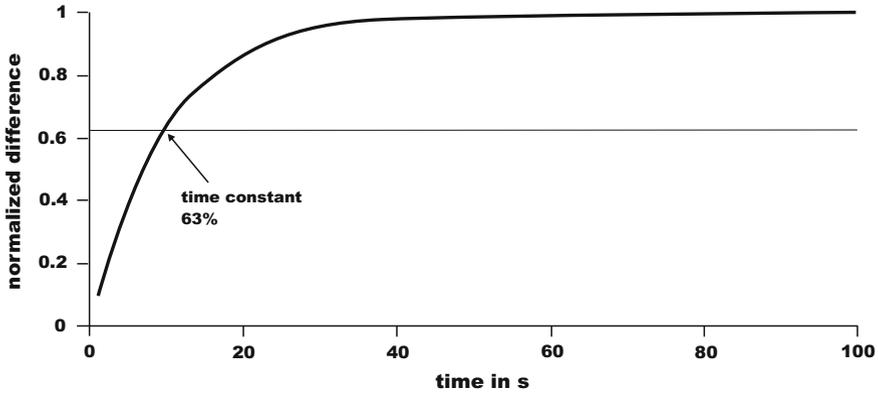
Fig. 6.5 Schematic graph for the documentation of the time constant for a change of the measured signal by a normalized signal difference

be defined, which allows comparing the time performance of different anemometers independent of wind speed:

> The distance constant is the length of the wind path necessary for the anemometer to reach 63% of the final velocity.

The relation between the time constant and the distance constant L can be calculated with the final velocity V_∞:

$$L = V_\infty \cdot \tau \tag{6.10}$$

6.1.4.3 Dynamic Error

The time constant describes the dynamic error of a measurement system. The typical case in meteorology of dynamic errors is, when a nearly linear change of the meteorological element occurs over a given time span. Instead of a change in time, a change in space is also possible which is typical for moving measurement systems such as radiosondes and tethersondes. For this case, Eq. (6.8) can be written in the form (Brock and Richardson 2001):

$$a \cdot t = X_i(t) + \tau \, \frac{dX_i}{dt} \tag{6.11}$$
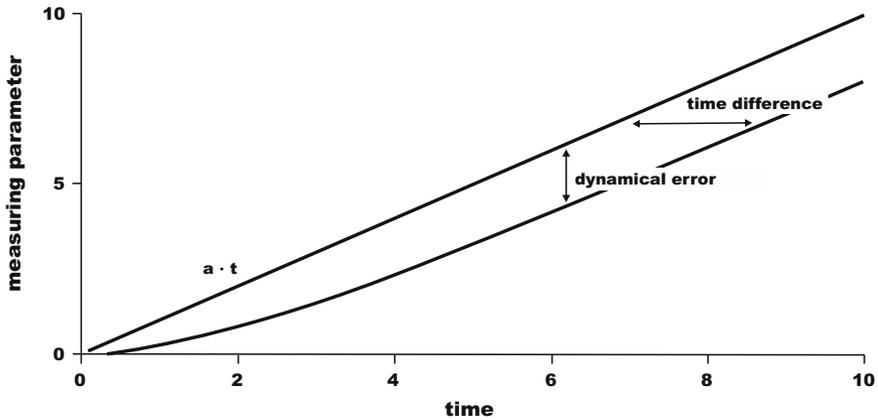
Fig. 6.6 Schematically graph of the dynamical error and of the time difference by a linear change of the input signal

The solution of this equation is:

$$X(t) = a\,t - a\,\tau\left(1 - e^{-\frac{t}{\tau}}\right) \tag{6.12}$$

The second term on the right-hand-side in Eq. (6.12) is responsible for the lag in the measured signal relative to the input signal and is called dynamical error:

$$\Delta X_d(t) = a\,\tau\left(1 - e^{-\frac{t}{\tau}}\right) \tag{6.13}$$

In the case of an input signal linearly varying with time, the output signal is shifted in relation to the input signal by the time difference $\Delta t = \tau$. The dynamic error is schematically shown in Fig. 6.6. Often dynamic errors are a reason for hysteresis.

For known input signal functions, the dynamic error can be easily corrected either mathematically or by correction networks. This may be relevant for the exact determination of the temperature gradient of an inversion layer of small vertical thickness. For measurements near the earth's surface this was also demonstrated for vertically (Mayer et al. 2009) and horizontally (Hübner et al. 2014) moving measurement systems.

6.2   Measurement of Meteorological Elements

Measurements in the atmosphere are different to other media, because of the influence of the wind field. Thus, atmospheric measurements are not point measurements. Rather turbulent eddies are measured, which move within a certain time

interval through the measurement volume. These eddies originate on the windward site of the sensor and can be attributed to a certain source area. These source areas are quite large for scalars and for fluxes their dimension is still of the order of 100 times the measurement height. Their exact determination is possible with footprint models (see Sect. 3.4). Consequently, some requirements for meteorological measurements are necessary.

Standard measurements in meteorological networks are made according to the international guide of the World Meteorological Organization (WMO 2008). Often, such regulations are extensive in order to guaranty a high and constant data quality for climate and environmental monitoring stations (see Appendix A.6). In contrast, at weather stations, which supply only data for weather forecasts or for the current weather state (nowcasting), less accurate sensors can be used. Research and special practical applications require specialized measurement stations (VDI 2006), which are listed in Table 6.1. The typical parameters collected at such sites are given in Appendix A.6.

Micrometeorological measurements are related to the meteorological scales according to Orlanski (1975) (see Fig. 1.2). These relations are relevant as well for

Table 6.1 Classification of meteorological measurement stations (VDI 2006), except stations of meteorological services which are classified by WMO (2008)

Number	Indication	Feature
1	Agrometeorological station	Agrometeorological basic parameters e.g. for the determination of evaporation
2	Microclimatological or micrometeorological station	Miscellaneous application with different instrumentations, e.g. biometeorological measurements
3	Micrometeorological station with turbulence measurements	Including eddy-covariance measurements for research purposes
4	Air pollution stations	Determination of parameters for air pollution calculations; with additional meteorological measurements
5	Disposal site stations	Mainly for the determination of the water balance
6	Noise station	Determination of parameters (mainly wind) for the meteorological influence (ISO 1996)
7	Roadside station	Measurement of meteorological elements which may affect the traffic
8	Hydrological station	Mainly precipitation measurements
9	Forest climate station	Measurement of meteorological elements in clearing and below trees
10	Nowcasting station	Measurement of the actual weather state, e.g. with present weather sensors
11	"Hobby station"	Measurement of meteorological elements with simple sensors but according the relevant installation instructions

Table 6.2 Assignment of direct and remote sensing systems to meteorological scales (the grey shading shows the degree of scale assignment)

Sensor system	macro	meso			micro		
	β	α	β	γ	α	β	γ
Radio sonde	▓	▓					
Boundary layer sonde			▓	▓			
Tower > 100 m			▓	▓			
Mast < 50 m				▓	▓	▓	
Turbulence sensors					▓	▓	▓
Satellite (vertical resolved)	▓						
Wind profiler		▓	▓	▓			
Sodar			▓	▓			
RASS			▓	▓			
Lidar			▓	▓			

Table 6.3 Assignment of scales of models to the necessary resolution of input parameters (the grey shading shows the degree of scale assignment)

Resolving structures	macro	meso			micro		
	β	α	β	γ	α	β	γ
Horizontal fields	▓	▓	▓	▓			
Vertical distributions			▓	▓	▓	▓	▓
Boundary layer parameters		▓	▓	▓	▓	▓	▓
Specified surface layer parameters				▓	▓	▓	▓

both in situ and remote sensing measurement techniques (Table 6.2). In the case of in situ techniques the sensor mast determines the scale.

Knowing the scale of the measurement systems is very important if the data are used as input parameters of models. The smaller the scales of the models, the greater the importance of vertical structures, boundary layer structures, and soil layer conditions (Table 6.3).

6.2.1 Radiation Measurements

Most radiation sensors are based on the principle of a radiation-caused heating and therefore an increase of the surface temperature of a receptor. For absolute devices (used for calibration) the temperature is directly measured on a black receiver

surface, which is irradiated without any filters directly by the sun. Due to the selective measurement of the direct sun radiation, the longwave radiation can be neglected, and therefore absolute devices measure only the shortwave radiation. Relative devices measure the temperature difference between two different irradiated areas one black and one white. Nowadays, silicon sensors are also available. Furthermore radiation sensors are classified depending on if they measure radiation from the half space or directed (from the sun) and if they measure short or long wave radiation. For measurements of the short wave diffuse radiation the sun is shadowed. Net radiometers measure the upper and lower half space. The possible spectral range can be selected by the material, which is used for the dome (receiver protection). Domes made of quartz glass are only permeable for short wave radiation (0.3–3.0 µm). For measurements of short and longwave radiation (0.3–100 µm) domes with Lupolen (special polyethylene) are used, and for longwave radiation (5.0–100 µm) domes made from silicon are used. The spectral gap region (3.0–5.0 µm) is accounted for in the calibration of the longwave radiation sensors but it has no significant influence on the measurements due to the low amount of energy in this range. Using a special set of filters or spectrally sensitive photo-electric cells, the photosynthetic active radiation (PAR) can be measured. PAR has dimensions of $\mu mol\ m^{-2} s^{-1}$, and the numerical value is approximately twice the numerical value of the global radiation in Wm^{-2}. Radiation instruments working in the small or large atmospheric window of the longwave range and a relatively small dihedral angle are used for measuring surface temperature. An overview is given in Table 6.4.

Table 6.4 Classification of radiation sensors

Measurement device	Sensor type		Wave length		Opening angle	
	absolute	relative	short wave	long wave	half space	directed
Absolute radiometer	x		x			x
Pyrheliometer		x	x			x
Pyranometer		x	x		x	
Albedometer		x	x		x[a]	
Pyrgeometer		x		x	x	
Net pyrgeometer		x		x	x[a]	
Radiometer		x	x	x	x	
Net radiometer		x	x	x	x[a]	
PAR radiation sensor		x	x (partly)		x	
IR radiation thermometer		x		x		x

[a]upper and lower half space

Table 6.5 Quality requirements for pyranometers (ISO 1990; WMO 2008), percents are related to the full measurement range

Property	Secondary standard	First class	Second class
Time constant (99%)	<15 s	<30 s	<60 s
Offset (200 W m^{-2})	±10 W m^{-2}	±15 W m^{-2}	±40 W m^{-2}
Resolution	±1 W m^{-2}	±5 W m^{-2}	±10 W m^{-2}
Long term stability	±1%	±2%	±5%
Non-linearity	±0.5%	±2%	±5%
Cosine response 10° solar elevation, clear	±3%	±7%	±15%
Spectral sensitivity	±2%	±5%	±10%
Temperature response	±1%	±2%	±5%

In the last 15–20 years, remarkable progress was achieved regarding the accuracy of radiation sensors. This success is based on the classification of radiation sensors by the World Meteorological Organization (Kasten 1985; WMO 2008) with clear guidelines for the error limits (Table 6.5) and also on the creation of the Basic Surface Radiation Network (BSRN) of the World Climate Research Program with a well-formulated quality control scheme (Gilgen et al. 1994; Ohmura et al. 1998). Therefore, the world radiation centre in Davos (Schwitzerland) maintains a collection of sensors called the World Radiation Reference. The other world centers regularly compare their Primary Standard devices (ISO 1990) with this reference. Regional and national radiation centres should compare their Secondary Standard devices with the world centres at least every 5 years. Currently, the widely used pyranometers PSP (Eppley Lab. Inc., USA), CM11, and especially CM21 (producer: Kipp & Zonen, The Netherlands) conform to the Secondary Standard.

For radiation sensors, a cosine correction is of special importance because the radiation power does not exactly follow the cosine of the solar angle of incidence. The reasons for the corrections are the unequal thickness of the domes and the changing thickness of the atmosphere with changes of the angle of incidence. Therefore, the exact horizontal levelling of the sensor and the clearness of the domes should be controlled.

In any case, the radiation instruments should be permanent (1–3 years) compared with national sensors for comparison (etalon). Because Secondary Standard devises are widely used, the comparisons with the sensors of different users are possible.

In contrast to shortwave radiation sensors, longwave radiation sensors are insufficiently calibrated. Serious differences were pointed out by Halldin and Lindroth (1992). While shortwave radiation sensors can be calibrated relatively easily against sun or with a lamp of defined radiation, calibration of longwave radiation sensors requires that radiation of the sensors themselves must be taken into account. The measured signal is simply the difference between the incoming longwave radiation and the longwave radiation of the housing in the form

$$I \downarrow = \frac{U_{rec}}{C} + k\sigma_{SB}T_G^4, \tag{6.14}$$

where U_{rec} is the voltage measured at the receiver, C and k are calibration coefficients, and T_G is the housing temperature which must be measured.

Progress in sensor development was made by Philipona et al. (1995), who installed thermistors in the silicone domes of the longwave radiation sensor to measure the temperature of the dome to correct the effects of dome temperature and local heating by shortwave radiation. The correction requires the temperatures of the housing and the dome (T_D):

$$I \downarrow = \frac{U_{rec}}{C}\left(1 + k_1\sigma_{SB}T_G^3\right) + k_2\sigma_{SB}T_G^4 - k_3\sigma_{SB}\left(T_D^4 - T_G^4\right) \tag{6.15}$$

To take into account the influence of the shortwave radiation, the so-called *f*-correction (Philipona et al. 1995) is added in Eq. (6.15), where the temperature differences between the North and South, North and Southeast, and North and Southwest sides of the dome must be considered. The *f*-correction is nowadays not very often applied because the accuracy of the temperature measurements is not good enough and cross-sensitivities occur. Good pyrgeometers can reach an accuracy of ± 2 Wm^{-2} if they are carefully calibrated according to Eq. (6.15) (Philipona et al. 2001), which is comparable with the characteristics of pyranometers.

In micrometeorology, net radiation measurements are highly relevant, and thus a high accuracy is required. Instead of the formerly used radiometers, which measured the short and longwave radiation together, sensors that measure all four radiation components are now quite common (Fig. 6.7). Of special importance is the ventilation of the sensor such that the body temperature, which is measured with a temperature sensor (Eq. 6.14), is uniform. As an additional effect, the ventilation averts dew formation on the calottes, which tampers the radiation fluxes in the morning hours.

Fig. 6.7 Net radiometer CNR4 with two as albedometer installed pyranometern (*right*) and pyrgeometern (*middle*) and a common ventilation (published with kind permission of © Kipp & Zonen, All rights reserved)

Net radiometer measurements must also meet some requirements regarding the underlying surface: It should be homogeneous to avoid errors it should reflect or emit the entire radiation from the lower half space. According to Latimer (1972), for an installation height of 2 m 90% of the radiation comes from a circle with a 12 m diameter, 95% from a circle of 18 m diameter, and 99% from a circle of 40 m diameter. This relationship is linear and the proportionality factor between the measurement height and the diameter of the circle is 6, 9, and 20.

6.2.2 Wind Measurements

Classical wind measurement devices are based on a mechanical principle, where the wind path is transformed into a rotation movement. Over the last 10 years, the application of ultra sonic anemometers that transmit and receive sound signals have become more common and have started to replace traditional rotation anemometers. Also remote sensing methods with e.g. radar became more widespread. The sensors can be further classified based on whether they can be used for standard measurements or for turbulence measurements using the eddy-covariance method. An overview is given in Table 6.6.

For mechanical anemometers (Fig. 6.8), the knowledge of the transfer function between the velocity in a wind tunnel and the velocity measured with the anemometer is of high importance, which must be determined in the wind tunnel (ISO 2007):

> The transfer function is the linear dependence between the wind velocity and the rotation velocity of the anemometer within a defined working range.

This calibration relation is linear over a wide range of velocities, but for low velocities (<2–4 ms^{-1}) is exponential. This is shown in Fig. 6.9 where c is the threshold velocity, which should not be confused with the intersection of the linearly extrapolated transfer function to the point with zero revolutions, a:

Table 6.6 Classification of wind sensors (anemometer)

| Type of sensor	Measurement principle				Application	
	Mech.	Sound	Therm.	Other	Mean	Turb.
Cup anemometer	x				x	
Propeller anemometer	x				x	(x)
Hot wire anemometer			x			x
Sonic anemometer		x			x	x
Laser anemometer				x	(x)	x

Fig. 6.8 Cup anemometer (published with kind permission of © Th. Friedrichs & Co., Schenefeld near Hamburg, All rights reserved)

> The threshold velocity of a rotating anemometer is the lowest wind speed that transfers the rotating anemometer into a continuous movement.

Beyond the threshold velocity (about 0.1–0.3 m s^{-1}), the so-called distance constant is important. It is a measure of inertia, and gives the necessary wind path required for an anemometer to register 63% of a wind velocity difference (see Sect. 6.1.4.2). The distance constant is an important parameter for mechanical anemometers; for sensitive propeller anemometers it is about 1 m; for small cup anemometers it is about 2–3 m, and for larger anemometers it is about 5 m. Note that sonic and hot wire anemometers in the usual application range are free of inertia. The distance constant should be used for the assessment of the measurement quality instead of the threshold velocity, because the starting velocity is generally within a range below 0.5–1.0 ms^{-1}, where the turbulent wind field is not fully developed.

In a turbulent flow, additional problems for mechanical anemometers exist (Kristensen 1998). With increasing distance constant, the wind velocity will be overestimated due to the mechanical inertia (over speeding):

> Overspeeding is the turbulence-caused over estimation of the measured wind velocity relative to the true wind velocity.
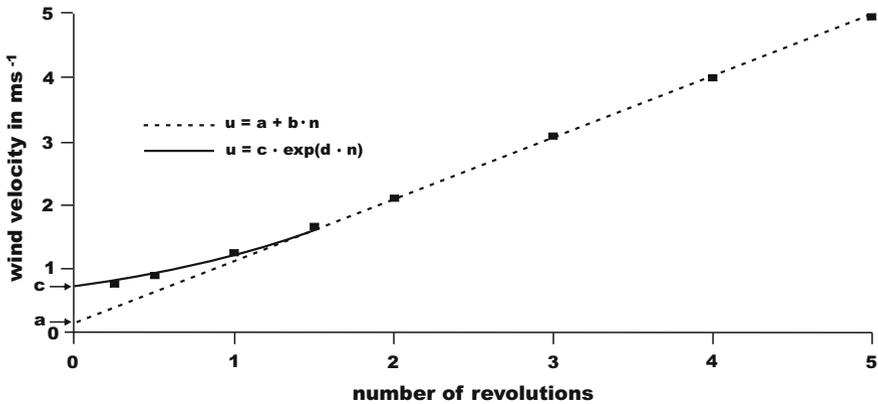
Fig. 6.9 Transfer function of a cup anemometer (VDI 2000) with n: number of revolutions of the anemometer, u: wind velocity and a, b, c and d: constants. Adapted with kind permission of © VDI e.V. and Beuth-Verlag, Berlin 2000, All rights reserved

Wind gusts will bring a mechanical anemometer into high rotation; however, after the gust the anemometer will require some time to adjust to the lower wind speeds. There is no compensation of these additional rotations in the case of low wind speeds. Overspeeding can be as large as 10% of the wind velocity, and is particularly large for low wind velocities and high distance constants. The value is proportional to $(\sigma_u/u)^2$. For micrometeorological measurements it is especially important that the overspeeding is small because otherwise wind gradients near the ground will be inaccurate.

The cosine response of an anemometer is of importance:

> The cosine response is the ratio of the measured wind velocity for a special angle of incidence to the wind velocity of the horizontal wind field multiplied by the cosine of the angle.

$$F(\alpha) = \frac{u(\alpha)}{u(0) \cdot \cos \alpha} \tag{6.16}$$

An ideal cosine response is given by $F(\alpha) = 1$. For propeller anemometers, deviations up to 15% occur for incidence angles of about 45° (Figs. 6.10 and 6.11). These deviations can be relatively simply corrected with the relation:

$$u_{korr}(\alpha) = u_{mess}(\alpha) \cdot [\cos \alpha - a \cdot \sin(2\alpha)] \tag{6.17}$$

where $a = 0.085$ (Drinkov 1972) or $a = 0.140 - 0.009\,u$ (Foken et al. 1983). For crosswinds, a dead zone of approximately $\pm 2°$ exists where the propeller does not
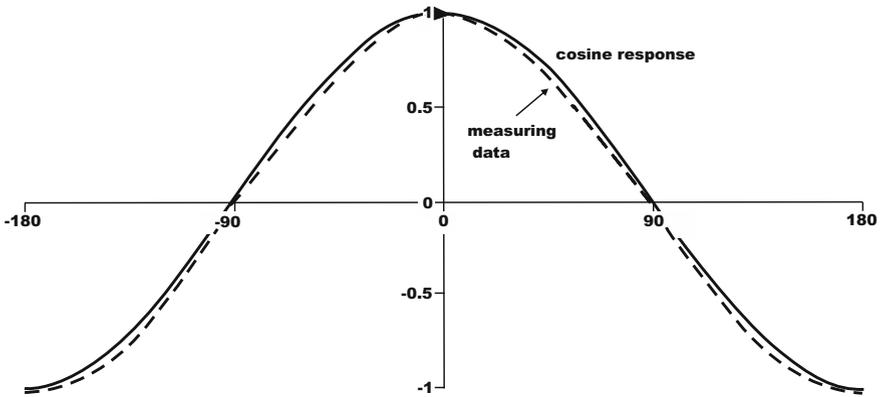
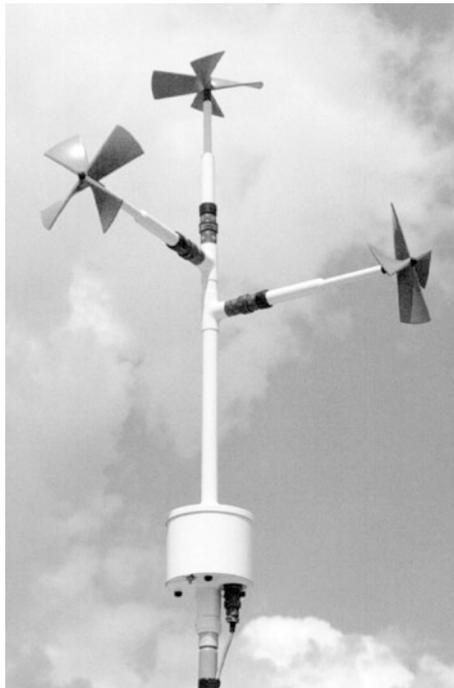**Fig. 6.10** Cosine response of a propeller anemometer

Fig. 6.11 UVW three-component propeller anemometer by Gill, model 27005T (published with kind permission of © R. M. YOUNG Company/GWU-Umwelttechnik GmbH, All rights reserved)

rotate. For measurements of the vertical wind, the dead zone is overcome with two inclined sensors. A shank extension is recommended for flow from the front (Bowen and Teunissen 1986) so that the dynamical conditions of a propeller for flow from the front and behind are nearly identical.

For cup anemometers, a cosine response cannot be assumed. If the inclination of the flow is not very great, then nearly the same wind velocity is always measured. This means that for an inclined flow the cup anemometers overestimate the wind velocity (Brock and Richardson 2001).

The first sonic anemometers used the phase shift method (Bovscheverov and Voronov 1960; Kaimal and Businger 1963). In this method, the ultrasonic signal of the transmitter is received at several points, and the phase difference between the transmitted and received signals is a function of wind velocity. The disadvantage of this method is that for different wind velocities (5–10 ms^{-1}steps) identical values will be observed, but the sound wave is shifted several times of 2π.

Modern sonic anemometers use the travel time principle and a direct time determination (Hanafusa et al. 1982). In this method, a sonic signal (about 100 kHz) is transmitted from both sides of a measurement path and received on the opposite sides. Due to the wind velocity, one signal is faster than the other. The exact travel times of the sonic signals are used for the determination of the wind velocity:

$$t_{1,2} = \frac{\sqrt{c^2 - u_n^2} \pm u_d}{c^2 - u^2} \, d \qquad (6.18)$$

where d is the path length, u_d is the wind component along the path, u_n is the normal component of the wind, and c is the sound speed. This relation is based on the assumption that the flow in the sonic anemometer is generally slightly shifted by an angle γ from the measurement path (Fig. 6.12), and for the travel times follows (Kaimal and Finnigan 1994; Brock and Richardson 2001):

$$t_{1,2} = \frac{d}{c \, \cos \gamma \pm u_d} \qquad (6.19)$$

The difference of the reciprocal travel times gives the wind velocity and the sum of the reciprocal travel times gives the sound velocity:
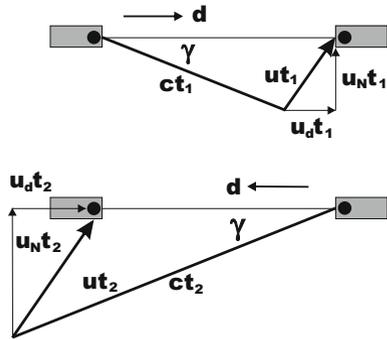
$$\frac{1}{t_1} - \frac{1}{t_2} = \frac{2}{d} \, u_d \qquad (6.20)$$

$$\frac{1}{t_1} + \frac{1}{t_2} = \frac{2}{d} \, c \sqrt{1 - \frac{u_n^2}{c^2}} \approx \frac{2}{d} \, c \qquad (6.21)$$

The first sonic anemometers with the travel time principle (Mitsuta 1966) could only measure the time difference. Measuring the wind velocity depended on the sound velocity and therefore on the temperature and the moisture:

$$c^2 = 403 T (1 + 0.32 \, e/p) \qquad (6.22)$$

Fig. 6.12 Vector graph of
the sound paths of a sonic
anemometer

From this equation the so-called sonic temperature can be calculated (Kaimal
and Gaynor 1991), which is similar to the virtual temperature:

$$T_s = T(1 + 0.32e/p) = \frac{d^2}{1612}\left(\frac{1}{t_1} + \frac{1}{t_2}\right)^2 \qquad (6.23)$$

A recalculation into the true temperature is possible by applying the geometric
parameters of the sonic anemometer (see Sect. 4.2.3.5).

Initially, the measurement paths of the sonic anemometers were predominantly
Cartesian orientated (Mitsuta 1966; Hanafusa et al. 1982). Modern sonic
anemometers have increased angles of the measurement paths, e.g. 120° (Fig. 6.13)

Fig. 6.13 Sonic anemometer
CSAT3 (Campbell Sci. Inc.)
with inclined measurement
paths and large inflow sector;
additionally an IR gas
analyzer LI7500 (Li-Cor) is
mounted (*Photograph* Foken)
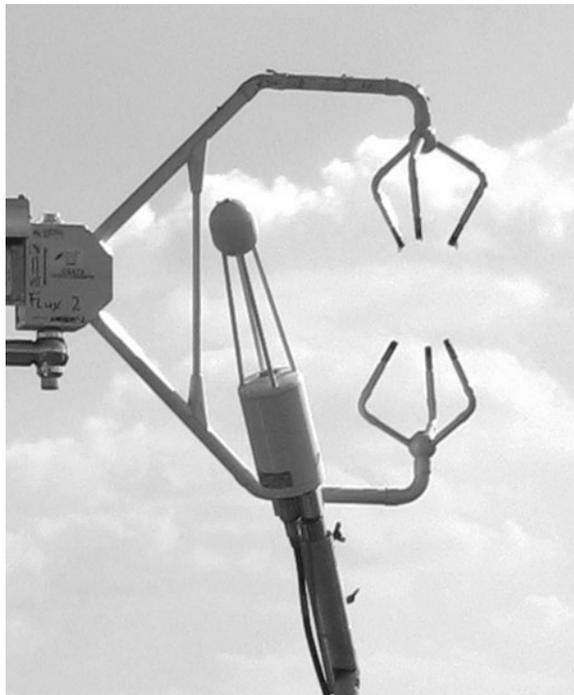
Fig. 6.14 Sonic anemometer
USA-1 with inclined paths
and omni-directional
construction (published with
kind permission of © METEK
GmbH, Elmshorn, All rights
reserved)

so as to get lower flow distortion. Also, sensors were developed, which can be used
for all flow directions (omni-directional, Fig. 6.14). A problem yet to be investi-
gated, is the significant self-correlation of the Cartesian wind components from the
inclined wind components, which influences the statistical independence for the
calculation of the covariances.

The calibration of sonic anemometers is very stable. However, before the
application a zero-point test should be done in a closed chamber (ISO 2002). Due to
the construction of the anemometer a reduction of the wind field is possible. In a
turbulent flow, the errors due to flow distortion are often smaller than those for the
laminar flow in the wind tunnel. Therefore, the application of the wind tunnel
correction may lead to an overcorrection. For flux measurements, it is important that
there are no sensor mountings below the measurement path for the vertical wind
component, otherwise flow corrections up to 10% are possible. For more details see
Sect. 4.2.3.2.

The number of different sonic anemometer types has increased in the last few
years. Thus, a type of classification is necessary, which is given in Table 6.7. The
accuracy is not only dependent on the type of the sonic anemometer but also on the
turbulent flow field. This influence can be taken into account by data quality
investigations (see Sects. 4.2.5, 4.2.7, and Table 4.14).

Table 6.7 Classification of sonic anemometers (based on a classification by Foken and Oncley 1995; Mauder et al. 2006)

Anemometer class		Sensor type
A	Basic research	Kaijo-Denki typ A Campbell CSAT3, Gill HS
B	General use for flux measurements	Kaijo-Denki typ B Gill Wind Master, R2, R3 METEK USA-1, Young 81000
C	General use for wind measurements	Sensors of class B 2D-anemometer of different producers

6.2.3 Temperature and Humidity Measurements

6.2.3.1 General Statements

The classical mercury thermometers (recently liquid-in-glass thermometers with alcohol), bimetal thermometers, and hair hygrometers have mostly been replaced by electrical measurement principles. The measurement of electrical resistance is used most frequently for temperature measurements. Thermocouples and thermistors are reserved mostly for special measurements with small sensors. Due to the temperature sensitivity of the sound velocity, sonic anemometers are often used for temperature measurements (remark: the sonic temperature is not absolutely equal to the temperature, see Sect. 4.2.3.5). For humidity measurements, ceramic material or polymers are used to measure the relative humidity, and optical techniques are used to measure the absolute humidity. The dew point temperature is measured by detecting condensation on a chilled mirror. An overview is given in Table 6.8

Table 6.8 Classification of temperature (T) and humidity sensors (H)

Type of sensor	Measurement principle				Application	
	Therm.	Electr.	Optical	Other	Mean	Turb.
Psychrometer (T,H)	x	x			x	
Liquate-in-glass thermometer (T)	x				x	
Bimetal thermometer	x				x	
Resistance thermometer (T)		x			x	(x)
Thermistor (T)		x			x	
Thermocouple (T)		x			x	(x)
Sonic thermometer (T)				x	x	x
Hair hygrometer (H)				x	x	
Capacity hygrometer (H)		x			x	
Dew point hygrometer (H)		x		x	x	
Infrared hygrometer ((H)			x		(x)	x
Ultraviolet hygrometer (H)			x			x

Table 6.9 Time constant of
temperature and humidity
measurement systems

Type of sensor	Time constant in s
Sonic thermometer	<0.01
Optical humidity measurement system	<0.01
Thin resistance wires (<20 μm)	<0.01
Thermocouples (<20 μm)	<0.01
Thermistors	0.1–1
Resistance thermometers	10–30
Liquate-in-glass thermometers	80–150

where it is also indicated if the sensor can be used for the observation of mean or
turbulent quantities.

An important parameter for temperature and moisture sensors is the time constant (see Sect. 6.1.4.1). Typical time constants are given in Table 6.9. It is seen that
the wet sensors (e.g. at a psychrometer) are less inert than dry sensors.

6.2.3.2 Temperature Measurement

Accurate measurements of the true air temperature are one of the most challenging
problems in meteorology. Even today, it is worth reading the paper by Albrecht
(1927). While improved technical possibilities are available, the measurement
problems are often significantly underestimated. Because temperature sensors warm
if they are exposed to radiation, they work better as a radiation sensor than a
temperature sensor. Therefore, at least the incidence of direct solar radiation on the
sensor must be eliminated. Furthermore, the thermometer must be ventilated to
prevent heating and to promote turbulent exchange of heat. Both of these
requirements are realized (ideally) with Assmann's aspirated psychrometer
(Assmann 1887, 1888; Sonntag 1966–1968, 1994). The device consists of two
thermometers ventilated at a rate >2.5 ms^{-1} and equipped with a double radiation
shield. There are several duplicated sensors available, whereby not all have the
quality of the original sensor. Even electrical versions of the sensor are most
accurate if Assmann's dimensions of the double radiation shield are met and if the
ventilation velocity is larger than 2.5 ms^{-1} (Fig. 6.15, Frankenberger 1951).

Given the difficulties in measuring temperature, measurement accuracy outside
of closed rooms is typically about 0.1 K, and only for very well maintained devices
the accuracy can reach 0.05 K. Therefore, the errors due to radiation and turbulence
conditions are much greater than the possibilities of the recent electrical measurement techniques (<0.001 K).

The radiation influence on the temperature measurement is called radiation error
and can be estimated as an additional heating by the absorption of radiation by the
sensor. This heating depends on the Prandtl number,

$$Pr = v/a_T \tag{6.24}$$

which is the ratio of the kinematic viscosity to the molecular thermal conductivity and has the value 0.71 for air; the Reynolds number (Eq. 2.20), which is the ratio of inertial forces to frictional forces (see Sect. 2.1.2); and the Nusselt number,

$$Nu = f(Re, Pr) \tag{6.25}$$

which is a function of the heat conductance and the flow characteristics. The radiation error is therefore a function of the radiation balance at the sensor surface Q_s, the sensor surface area F, and the heat transfer properties, α,
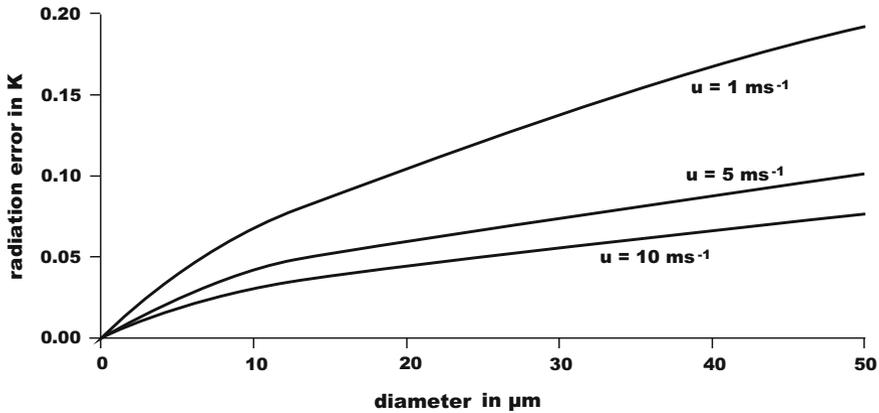
$$Sf = \frac{Q_s}{\alpha F} \tag{6.26}$$

where

$$\alpha = \frac{Nu\,\lambda}{d}, \tag{6.27}$$

$$Q_s = a\,K \downarrow F_R, \tag{6.28}$$

and a is the absorption capacity of the surface, λ is the molecular heat transfer number, d is the sensor length, and F_R is the area affected directly by the radiation.

Fig. 6.16 Radiation error of thin platinum wires for $K\downarrow$ = 800 W m^{-2} and a = 0.5 (adapted from Foken 1979, with kind permission of © Wiley-VCH, Weinheim 1979, All rights reserved)

For forced convection ($0.01 < Re < 10{,}000$) it follows (van der Hegge Zijnen 1956) that:

$$Nu = 0.42\,Pr^{0.2} + 0.57\,Pr^{0.33}Re^{0.5}$$
$$Nu_{air} = 0.39 + 0.51\,Re^{0.5} \tag{6.29}$$

For the absorption capacity of platinum (a = 0.5), the radiation errors are given in Fig. 6.16. Thus, radiation errors below 0.1 K are realized only for wire diameters <20 μm.

The radiation error can be excluded only for very thin and spread-out resistance wires and for thermocouples of the same dimension. The use of thin resistance wires for turbulence measurements is based on Kretschmer (1954). Extensive investigations of the use of resistance wires were made, for example, by Tsvang (1960), Foken (1979), and Jacobs and McNaughton (1994). For thin platinum wires, it must be taken into consideration that the specific resistance in $\Omega \cdot$ m for diameters <50 μm, but especially for diameters <10 μm, increases because the diameter is in the order of the free path length of the electrons. Such sensors are nowadays commercially no longer available.

For the measurement of the mean temperature, a suitable radiation shield, e.g. double protection tube or weather hut with double Venetian blind, is necessary to reduce the radiation error. Huts have the disadvantage that they heat up, and the so-called hut error of up to 1 K can occur (WMO 2008). For micrometeorological measurements, small cylindrical huts designed by Gill (Fig. 6.17) are often used. These huts were described regarding their dynamic and radiation properties by Richardson et al. (1999). The hut error can be removed by sufficient ventilation. Therefore, the Reynolds number should be above the critical Reynolds number to achieve a turbulent flow:

Fig. 6.17 Temperature hut according to Gill (model 41003) for micrometeorological investigations (published with kind permission of © R. M. YOUNG Company/GWU-Umwelttechnik GmbH, All rights reserved)

$$\text{Re} = \frac{L\,V}{v} \geq \text{Re}_{krit} = \begin{pmatrix} 2300 & \text{tube} \\ 2800 & \text{plate} \end{pmatrix} \tag{6.30}$$

Below the critical Reynolds number, a laminar flow occurs near the sensor, and increases the response time of the measurement. The laminar flow boundary layer is thinner than the molecular temperature boundary layer (von Driest 1959):

$$\frac{\delta}{\delta_T} = \sqrt{Pr} = 0.85 \ \ (\text{air}) \tag{6.31}$$

Except for thermocouples, platinum wires have prevailed over all other temperature measurement sensors because of the stable temperature-resistance dependency. The resistance can be determined with the following equation

$$R(T) = R(0°C) \cdot \left(1 + \alpha T + \beta T^2\right), \tag{6.32}$$

Table 6.10 Maximal differences for 100 Ω platinum resistance thermometers (DIN-EN 2009)

Temperature °C	Maximal difference					
	Class A		Class B		Class AA[a]	
	K	Ω	K	Ω	K	Ω
−100	±0.35	±0.14	±0.8	±0.32	±0.27	±0.11
0	±0.15	±0.06	±0.3	±0.12	±0.10	±0.04
100	±0.35	±0.13	±0.8	±0.30	±0.27	±0.11

[a]formerly class 1/3 class B

where α is a temperature-dependent coefficient which ranges from 0.00385 to 0.00392 K^{-1} depending on the purity of the platinum. By adding iridium, the brittleness of the wire can be reduced so that lower temperature coefficients are typical. Under these circumstances β is about $-5.85 \cdot 10^{-7}$ K^{-2}. In the meteorological measurement range of –50 to 50 °C nearly linear temperature dependence is obtained. Typically, platinum thermometers are produced with a resistance of R (0 °C) = 100 Ω (1000 Ω is also available). The quality of resistance thermometers in Germany and other countries is standardized (DIN-EN 2009). The sensors are separated into classes A, B, and AA (Table 6.10), where selected resistance thermometers with differences of only 1/3 or 1/10 of the DIN-class are also available. Regularly, thermometers are used with class AA, formerly 1/3 DIN class B, which is better than class A.

The electrical measurement of the resistance is made with bridge circuits. The classical Wheatstone bridge with two and three wire circuits is seldom used because of non-linearity and a poor compensation for wire resistances. Recently, e.g. Thompson bridges or constant- current sources with four-wire circuits are used.

The progress of resistance measurements using integrated electronic circuits, has widely replaced the thermistor (Rink 1961) as a measurement sensor, because even though it has a tenfold higher temperature sensitivity, it has nonlinear characteristics. Before its use, thermistor must undergo heat and quench ageing, and during operation frequent recalibrations are often necessary. The temperature dependence is given by

$$R(T) = R(0°C) \cdot e^{\left(\frac{\alpha}{T} + \frac{\beta}{T^3}\right)} \tag{6.33}$$

with typical values of $\alpha \sim 4500$ K and $\beta \sim -1.5 \cdot 10^7$ K^3 (Brock and Richardson 2001). The most important areas of application are radiosondes and the measurements of body and dome temperatures in radiation sensors.

6.2.3.3   Humidity Measurement

Assmann's aspirated psychrometers are most reliable devices for measuring humidity, and can also be used for comparison measurements (see Sect. 6.2.3.2).

This instrument has a second thermo-meter with a wet bulb for measuring the wet bulb temperature. Both thermometers must be ventilated with velocities $>2.5 \text{ ms}^{-1}$. It uses the effect of evaporative cooling. The water vapour pressure can be determined from the temperature difference between the dry (t) and wet (t') bulb temperatures using Sprung's psychrometric equation (psychrometer constant $\gamma = 0.666 \text{ hPa K}^{-1}$ for $p_0 = 1013.25 \text{ hPa}$, $t = 20 \text{ °C}$):

$$e = E(t') - \gamma \cdot \frac{p}{p_0} \cdot (t - t') \tag{6.34}$$

Meanwhile the improved relationship by Sonntag et al. (1989) is recommended by the World Meteorological Organization (WMO 2008) and widely applied. Above water follows

$$e = E(p, t') - 6.53 \cdot 10^{-4} \cdot p \left(1 + 9.44 \cdot 10^{-4} \cdot t'\right) \cdot (t - t'), \tag{6.35}$$

and above ice

$$e = E(p, t') - 5.75 \cdot 10^{-4} \cdot p \cdot (t - t'). \tag{6.36}$$

For wet temperatures above 30 °C a further modification is recommended (Sonntag et al. 1989):

$$e = E(p, t') - 6.53 \cdot 10^{-4} \cdot (p - E(p, t')) \cdot \left(1 + 9.44 \cdot 10^{-4} \cdot t'\right) \cdot (t - t') \tag{6.37}$$

For high accuracies, there are dew- and frost-point hygrometers. These expensive sensors can be used for comparison experiments (Sonntag 1994). In meteorological networks, capacitive sensors are widely used. These have replaced the hair hygrometer, which is still used for temperatures below 0 °C when the psychrometer has insufficient accuracy.

For many micrometeorological measurements of turbulent fluxes, the absolute humidity is necessary. For relative humidity sensors such as capacitive and hair hygrometers, the absolute humidity must be calculated with the temperature. This introduces temperature sensitivity, and makes temperature-independent humidity measurements impossible.

For the measurement of turbulent humidity fluctuations optical measurement methods are primarily used, which are based on the Lambert-Beer's law

$$I = I_0 \cdot e^{-k \cdot d \cdot \frac{c}{c_0}}, \tag{6.38}$$

where k is the absorption coefficient, d is the path length, and I_0 the radiation intensity at absorber concentration c_0. The measurement is made per unit volume. The measurement principle is schematically illustrated in Fig. 6.18.

The application of these techniques for turbulence measurements in the IR range are based on Elagina (1962) and in the UV range on Buck (1973), Kretschmer and

Fig. 6.18 Schematically
construction of an absorption
hygrometer
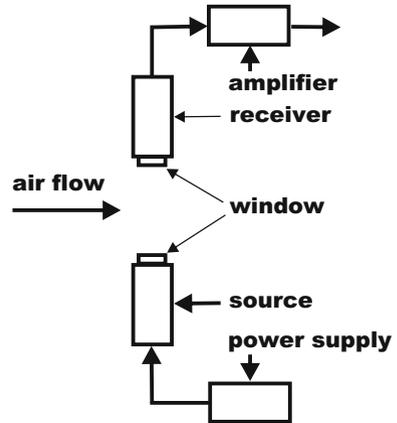
Karpovitsch (1973), and Martini et al. (1973). Many commercial developments
followed, which were summarized by Foken et al. (1995). Today, only commercial
sensors are used.

Instruments with either UV or IR radiation are used (Table 6.11). For mea-
surements of low absolute humidity instruments in the UV-range are preferred, and
for water vapour pressures larger than 10 hPa the IR-range is preferred. Due to the
low absorptivity of the IR-range relatively long (>0.12 m) measurement paths are
necessary. For a suitable wavelength, IR devices can also be used to measure
carbon dioxide concentration. The lifetime of UV devices is limited due to changes
of the lamp after about 1000 h. For these sensors, the surfaces of the optical
windows are treated with hygroscopic material such as magnesium fluoride, which
must be taken into account when the humidity is high. Therefore, IR hygrometers
have become the preferred instruments for many users and vendors. Besides the IR
open path systems (see Fig. 6.13), closed-path sensors, in which the air is with-
drawn near the sonic anemometer and measured some meters away in an IR
measurement cell are also applied (Leuning and Judd 1996; Moncrieff et al. 1997).
These systems have the benefit that density fluctuations do not occur if heated tubes
are used, and the WPL correction (see Sect. 4.2.3.6) can be dropped. However,

Table 6.11 Selected spectral lines for the water vapour absorption

Range	Wave length	Radiation source	Measurement length	Absorber
UV	0.12156 µm	Atomic hydrogen (Lyman-α)	3–10 mm	H_2O
	0.12358 µm 0.11647 µm	Krypton	5–15 mm	H_2O, (O_2, O_3)
IR	Different wave length	Stable electric light bulb	0.125–1 m	H_2O, CO_2

these are very complicated dynamical systems with low-pass characteristics. The time delay between the wind and concentration measurements is especially important and must be taken into account in flux calculations.

The calibration characteristics can change during the application time, and the devices working in the UV range are affected more than those in the IR range. Two calibration methods are commonly used: One method uses the calibration within a gas flow with a constant concentration of water vapour or other trace gases, and the other method uses a climate chamber. Also, the in situ calibration is possible by changing the path length for nearly constant background humidity (Foken et al. 1998; Foken and Falke 2012). This method works because according to Eq. (6.38) the trace gas concentration as well as the path length is in the exponent.

The application of very sensitive tuneable diode lasers (Edwards et al. 1994; Werle et al. 2008) increased during the last few years (e.g. Pattey et al. 2006; Sturm et al. 2012) because different gases such as methane, nitrogen oxides, and carbon isotopes can be measured and the instruments are now commercially available.

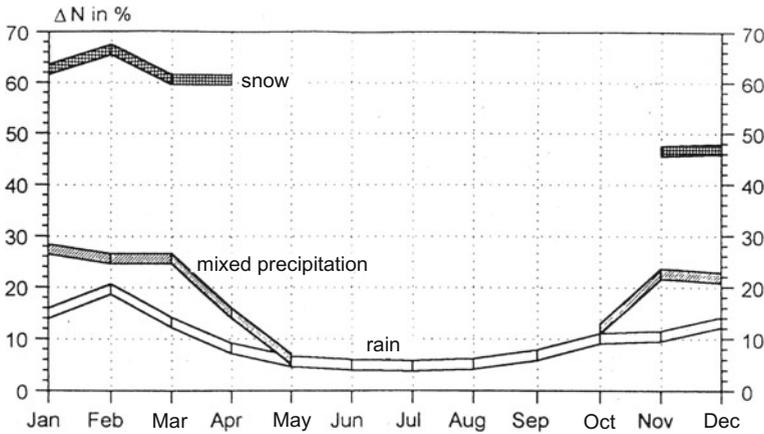### 6.2.4 Precipitation Measurements

Precipitation measurements are one of the standard meteorological measurement techniques. In Germany, the rain gauge according to Hellmann should have a 200 cm^2 collection area, but in other countries it is 500 cm^2. The daily emptying of a collection bucket is often replaced by automatic rain gauges. Various measurement principles are available. The tipping-bucket gauge collects a certain amount of water in a bucket, and when the full bucket tips it is emptied, and electrical signal is sent. The droplet counter counts the number of droplets of a uniform size. Recently, weight scale rain gauges are used; this type has the benefit that the danger of freezing is low. It should be noticed that the rain gauge according to Hellmann has a very adverse ratio of the wettable surface and the collection area (200 cm^2) with a value of 7.55.

Precipitation measurements play an important role in the calculations of the water balance. It should be noted that precipitation data listed in climatological tables are typically not corrected. The moisten error and the wind error (Sevruk 1981; Richter 1995) must be corrected. For solid precipitation, the wind error can be very large (Fig. 6.19). The correction equation for both errors is:

$$N_{korr} = N_{mess} + b\, N_{mess}^{\varepsilon} \tag{6.39}$$

The coefficients are given in Table 6.12. Correction values are for different seasons and regions in Germany (Richter 1995).

For wind exposure on slopes with 40% inclination, up to 10% more precipitation can be expected due to the increasing horizontal contribution. A calculation of this effect was presented by Junghans (1967)

Fig. 6.19 Measurement error of precipitation measurements (adapted from Richter 1995, published with kind permission of © Deutscher Wetterdienst, Offenbach 1995, All rights reserved)

Table 6.12 Coefficients of the precipitation correction according Eq. (6.43) according to Richter (1995)

Type of precipitation	ε	Horizontal shading (b-value)			
		2°	5°	9.5°	16°
Rain (summer)	0.38	0.345	0.310	0.280	0.245
Rain (winter)	0.46	0.340	0.280	0.240	0.190
Mixed precipitation	0.55	0.535	0.390	0.305	0.185
Snow	0.82	0.720	0.510	0.330	0.210

$$\frac{N_H}{N} = 1 + 0.113 \, tg \, g \, \sin A_j, \tag{6.40}$$

where N_H is the precipitation on the slope, N is the measured precipitation on a horizontal surface, g is the inclination of the slope, and A_j is the azimuth angle of the jth wind direction.

For accurate and comparable precipitation measurements, rain gauges should be protected by a wind screen and should be placed at a distance equal to at least four times the height of any nearby obstacles, (WMO 2008). Nevertheless, the absolute accuracy is hardly better than 5% and for single, low-intensity precipitation events it is even larger. Open questions concerning the accuracy of accumulated sums (month, year) remain even after field intercomparisons were conducted (Vuerich et al. 2009). However, the scatter of the single data indicates that systematic errors are rather small and the measurement error for most instruments are approximately 5–10%.

6.2.5 Remote Sensing Methods

Increasingly, remote sensing techniques are being used in micrometeorology and applied meteorology. The techniques use sound waves (Sodar), light (Lidar) or radio waves (RADAR), and by applying the Doppler effect the wind velocity can be measured remotely. The use of lasers and microwaves makes moisture measurements possible. These instruments do not provide reliable observations below 20–50 m above the ground, but for micrometeorologists they cover an important region of the atmospheric boundary layer. Additionally, in the lower atmospheric boundary layer scintillometers can be used to measure the structure functions of the refractive index over horizontal path lengths from which fluxes can be determined indirectly. The electromagnetic spectrum, which is used by the remote sensing methods, is summarized in Table 6.13.

6.2.5.1 Sodar-RASS

The development of profiling techniques using sound are based on Russian theoretical work on wave propagation in the atmosphere (e.g. Tatarski 1961), while the first Sodar devices (**So**nic **D**etecting **A**nd **R**anging) by Kallistratova (1959) and McAllister et al. (1969) were constructed and used. The measurement principle is based on the fact that a sound pulse emitted into the atmosphere will be backscattered by temperature inhomogeneities. The degree of backscatter is directly proportional to the temperature structure function parameter. The classical range for application of these "monostatic" Sodars was the detection of inversion layers for air pollution purposes. By calibration of theses devices, the determination of the sensible heat flux using Eq. (2.140) is possible.

Subsequently, the Doppler effect was explored as a way to measure the three-dimensional wind field. These investigations lead to bistatic devices, which have low vertical operation range, and monostatic devices with one vertical and two sloping antennae. The accuracy of these Sodars is in the range of mechanical sensors (Table 6.14). However, these measurements are volume averages, and the horizontal wind components are measured in different sampling volumes, which may be far apart at high altitudes. For the standard deviation of the vertical wind it was found that the high values are underestimated and the low values are overestimated; this can be corrected.

Table 6.13 Ranges of the electromagnetic spectrum, which are used for remote sensing techniques in the atmospheric boundary layer

Frequency/wave length	Description	Sounding technique
1–5 kHz	Sound	Sodar
100 MHz–3 GHz	Ultra short waves (VHF), decimetre waves (UHF)	RASS, windprofiler
3–30 GHz	Centimetre waves	Microwave scintillometer
0.3–3 μm	Visible, infrared	Lidar
0.8–5 μm	Infrared	Scintillometer

Table 6.14 Measurement range and accuracy of Doppler-Sodar and RASS systems (Neff and Coulter 1986)

Parameter	Max. height in m	Resolution in m	Accuracy
Horizontal wind velocity	1000	15–50	± 0.5 m s^{-1}
Vertical wind velocity	1000	15–50	± 0.2 m s^{-1}
Structure function parameter	1500	2–10	$\pm 30\%$
Temperature (RASS)	600	15–50	± 0.5 K
Boundary layer height	600	2–10	$\pm 10\%$
Sensible heat flux	500	15–50	± 50 W m^{-2}

Modern Sodars use a "phased-array" arrangement, where a large number of loudspeakers are triggered in such a way that the sound pulse can be emitted in any direction. Thus, ground echoes and obstacles can be excluded. Also, the emission of single frequency pulses can be replaced by a continuous multi-frequency emission. The sampling frequency must be chosen in such a way that the cross sensitivity to the humidity is minimal.

The combination of a Sodar and a RADAR (Fig. 6.20) makes the measurement of the temperature field possible (RASS: **R**adio **A**coustic **S**ounding **S**ystem). In the RASS system, a Sodar emits vertically an acoustic wave, which is observed by the radar. Using the propagation speed of the sound wave, the sound temperature can be determined with Eqs. (6.22). Periodic inhomogeneities (turbulence elements) can only be detected if their size is approximately half of the wavelength of the sounding signal (Bragg condition).

While Sodar and Sodar-RASS systems offer reliable data at heights as low as 10–30 m, wind profilers have their first values at larger heights. The boundary-layer wind profiler works in the UHF range and is still interesting for micrometeorological applications; however, the tropospheric wind profiler works in the VHF rang and gives little data below 500 m.

6.2.5.2 Lidar

Due to the availability of improved laser techniques Lidar devices (**Li**ght **d**etection **a**nd **r**anging) have become quite popular (Weitkamp 2005). Depending on the type

Fig. 6.20 Sodar-RASS system consistent on a "phased-array" Sodar (*middle*) and two radar antenna (published with kind permission of © METEK GmbH, Elmshorn, All rights reserved)

of Lidar, in addition to aerosol measurements, which can be used to determine the mixed layer height, also wind profiles can be measured with Doppler-type instruments. The resolution of Doppler Lidars is similar to those given in Table 6.14 for Doppler-sodar devices. The benefit in comparison to Sodar technique is the noise-free sounding, but the measurements fail in the case of cloud cover.

Of special interest for boundary layer investigations are ceilometers. These are relatively simple back-scatter Lidars with an infrared laser with a wavelength of 0.9 µm, which were primarily used to detect the height of the clouds. Additionally, boundary-layer height can be detected from the vertical gradient of the back-scatter intensity as the height, where the gradient shows the largest negative deviation (Hayden et al. 1997). This method, which was originally developed for Lidar devices, can be transferred to ceilometers (Münkel et al. 2007; Helmis et al. 2012). Therefore, operational weather services are able to continuously produce boundary layer heights more easily than from radio soundings (see Sect. 2.6.1)

6.2.5.3   Scintillometer

The so-called scintillometer (Hill et al. 1980; Hill 1997) measures the refraction structure function parameter, C_n^2, and offers a method for the determination of the sensible heat flux and the friction velocity (Wyngaard and Clifford 1978). The bases for this are Eqs. (2.137) and (2.140) as well as other parameterizations for the dependency of the sensible heat flux on the temperature structure function parameter, C_T^2. The friction velocity can be calculated from the inner scale of the temperature fluctuations (Hill and Clifford 1978). Temperature or humidity inhomogeneities (IR or microwave scintillometer) cause a scintillation of the measurement beam, which can be evaluated.

Essentially, scintillometers are separated into two classes (DeBruin 2002) the large aperture scintillometer (LAS) and the small aperture scintillometer (SAS). The latter instrument is commercially available as a displaced-beam small aperture laser scintillometer (DBSAS). The LAS works in the IR range, has a measurement path length of several kilometers, and can determine only the sensible heat flux. In contrast, the DBSAS works with two laser beams over a distance of about 100 m (Andreas 1989). These systems can determine also the path-length-averaged turbulence scale, which is associated with the energy dissipation according to Eqs. (2.110) and by using the TKE equation Eq. (2.42), the direct determination of the friction velocity is possible when a stability dependence is taken into account (Thiermann and Grassl 1992). Note that scintillometers are not able to determine the sign of the sensible heat flux. Additional measurements (temperature gradient) are necessary, if the sign cannot simply be determined by the daily cycle because possibly unclear situations can occur in the afternoon. Scintillometers have a sensitivity that is in the middle of the measurement path rather than near the transmitter and receiver. This must be taken into account for footprint analyses of the measurement sector (Meijninger et al. 2002). Both scintillometer types have been successfully used in long-term measurement programs (Beyrich et al. 2002;

DeBruin et al. 2002). Relatively new is the microwave scintillometer, which measures the humidity structure function parameter $C_q{}^2$, see Eq. (2.136), and has the possibility of determining the latent heat flux (Meijninger et al. 2002, 2006).

6.2.6 Other Measurement Techniques

From the micrometeorological point of view, parameters other than those discussed are of special interest. In this section, a short overview of important measurements is given. But in some cases, the study of additional literature is necessary (DeFelice 1998; Brock and Richardson 2001; Moene and van Dam 2014).

6.2.6.1 Measurements in the Soil

Soil temperature, soil moisture, and the soil heat flux are especially relevant micrometeorological parameters (see Sect. 1.4.2). The soil temperature is a standard measurement using water-protected thermometers at 5, 10, 20, 50, and 100 cm depth. Micrometeorological investigations often need an increase of the measurement density close to the surface, e.g. in 2 cm depth. The heterogeneity of the soil and the plant cover make the positioning of the sensors difficult.

The soil moisture as a control parameter for evaporation is of special importance. The most accurate version for measurement is still the gravimetric method, where the soil probe is made with a soil core sampler and the soil is weighted after drying at a temperature of 105 °C. The measured change in weight is equivalent to the gravimetric water content (θ_g). Using a cylinder of known volume the volumetric water content (θ_v) can be determined. For a conversion of both parameters, the knowledge of the bulk density of the soil (dry density ρ_b) is necessary (ρ_w water density):

$$\theta_v = \theta_g \frac{\rho_b}{\rho_w} \tag{6.41}$$

A special electrical method for dry soil is the use of gypsum blocks, which include electrodes for measuring the electric conductivity. However, these devices must be calibrated individually in the laboratory. Note that the gypsum blocks have a strong hysteresis between moistening and drying.

For not very dry soils, tensiometers are widely used for the determination of the soil moisture tension by capillary forces. This technique uses a fine porous ceramic cup filled with water and placed in good contact with the moist soil. A balance of water pressure develops between the inner and outer sides of the cup. Using a glass tube extended into the cup, the pressure can be measured directly or the tube is closed with a septum and the pressure is measured with puncture devices. The matrix potential, ψ, in the depth, L (distance between the middle of the cup and the top of the tensiometer) can be calculated by

$$\psi = \psi_0 + (L - L_{bubble}) \tag{6.42}$$

where L is reduced by the height of the air bubble, L_{bubble}, in the glass tube. The pressure measured in the bubble (negative) is expressed as a length (ψ_0). There is a soil-type specific and characteristic connection (water tension curve) between the matrix potential and the volumetric water content that is used for the calculation. The use of tensiometers is diminishing because of the effort needed for the measurements and the indirect calculation.

Widely used today, is the capacitive TDR-method (time domain reflection). The instrument consists of two or more electrodes separated 2–5 cm and placed into the soil. The dielectric constant is measured by the travel time of an electric wave in the medium. The reflection properties are influenced in a characteristic way by the soil moisture. Because the electrical field develops over a large soil volume, an absolutely exact determination of the measurement height is not possible. With this method only the volumetric soil moisture is measured.

Soil heat flux can be measured using soil heat flux plates. These consist of two metallic plates separated by a layer of resin, with a heat conductance matching the one of the soil. The temperature difference measurement between both plats is made with thermocouples, where according to Eq. (1.12) the output signal is proportional to the soil heat flux. The plates require calibration.

There are numerous sources of errors for the soil heat flux plates. Especially important are the differences of the heat conductivities between the plates and the soil and at the edges of the plates, which are insufficiently included in the temperature measurement (van Loon et al. 1998). The first published and widely used correction method is the Philip correction (Philip 1961). The correction factor f between the measured soil heat flux, Q_G', and the soil heat flux through the surrounding soil, Q_G, is given by

$$f = \frac{Q_G'}{Q_G} = \frac{\varepsilon}{1 + (\varepsilon - 1)H'} \tag{6.43}$$

where ε is the ratio of the heat conductivities $\lambda_{plate}/\lambda_{soil}$. The factor H is dependent on the geometry of the heat flux plate and is given for square plates as:

$$H = 1 - \frac{1.70T}{L} \tag{6.44}$$

and for round plates as:

$$H = 1 - \frac{1.92T}{D} \tag{6.45}$$

where T is the thickness of the plate, L is the length of the square plate, and D is the diameter of the round plate. The Philip correction is recommended by Fuchs (1986), but it is doubted by other authors (van Loon et al. 1998). Also different types of plates have significant differences (Sauer et al. 2002). By applying self- calibrating

heat flux plates (Hukseflux HFP01SC), which determine a correction value by using a short and well-defined heating, the Philip correction can be omitted (Liebethal and Foken 2006). In contrast, these sensors (Hukseflux HFP01SC and TF01) are however less suitable to determine the heat conductance and the volumetric heat capacity by in situ measurements.

Generally, for micrometeorological measurements only the soil heat flux at the surface is necessary. Therefore, according to Eq. (1.14) the storage term above the heat flux plate must be determined by additional temperature measurements. It is also possible to eliminate the heat flux plates, if in a certain depth according to Eq. (1.12) the heat flux can be determined from the temperature gradient. It is recommended to determine the temperature gradient or to locate the heat flux plates at a depth of 10–20 cm to reduce errors. Both methods (using soil heat flux plates or temperature gradients for determining the storage) have approximately the same accuracy in an undisturbed soil profile (Liebethal et al. 2005).

The volumetric heat capacity, necessary for the determination of the storage term, can be determined with the method of de Vries (1963)

$$C_G = C_{G,m} x_m + C_{G,o} x_o + C_{G,w} \theta, \tag{6.46}$$

with the heat capacity of the mineral and organic compounds ($C_{G,m} = 1.9 \cdot 10^6$ J m^{-3} K^{-1}, $C_{G,o} = 2.479 \cdot 10^6$ J m^{-3} K^{-1}) and for water ($C_{G,w} = 4.12 \cdot 10^6$ J m^{-3} K^{-1}). The contribution of mineral components (assumed mineral 2650 kgm^{-3}), x_m, and can be determined by volume measurements of the soil. For depths up to 20 cm, x_o can often be neglected. The volumetric moisture of the soil is θ and given in m^3 m^{-3} as is x_m.

For the calculation of soil heat flux from the temperature gradient, the coefficient of heat conductance, a_G, is necessary:

$$a_G = C_G v_T \tag{6.47}$$

where v_T is the thermal diffusion coefficient and C_G is given by Eq. (6.46).

The thermal diffusion coefficient can also be determined using the method by Horton et al. (1983), in which the temperatures sensors are installed at three depths (10, 15 and 20 cm) and the temperature difference between two time steps ($\Delta t = 1$ min) is determined:

$$\frac{T_{15cm}^{n+1} - T_{15cm}^n}{v_T \Delta t} = \frac{T_{20cm}^n - 2T_{15cm}^n + T_{10cm}^n}{(\Delta z)^2} \tag{6.48}$$

A relatively simple yet reliable approach (Liebethal and Foken 2007) for the determination of the soil heat flux was presented by Braud et al. (1993). It is based on a heat flux measurement at $z = 10$ cm depth and temperature measurements at 1 and 10 cm depth as well as an estimate of the soil moisture for the determination of the volumetric heat capacity:

$$Q_G(0,t) = Q_G(-z,t)$$
$$+ C_G z \frac{T_1(t) - T_1(t - \Delta t) + 0.5[\Delta T(t - \Delta t) - \Delta T(t)]}{\Delta t} \quad (6.49)$$

The time interval for such investigations is 10 min.

6.2.6.2 Soil Chamber Measurements

Ecologists use soil chambers to investigate the matter exchange between the atmosphere and the soil. With this method fluxes can be determined for very small plots. A good overview about this technique is given by Rochette and Hutchinson (2005). From the micrometeorological point of view these measurements are often criticized because of two reasons (Denmead 2008). First, chambers separate the near surface volume from the atmosphere such that typical atmospheric turbulent conditions are not present within the chamber and the longwave net radiation inside the chamber is nearly zero. Secondly, chamber measurements are often made manually and the daily cycle cannot be fully reproduced and the sampling theorem is not fulfilled. To overcome these problems, the chamber is often ventilated, but the typical wind profile of a boundary layer cannot be realized. Cooling pads are used to prevent overheating due to shortwave radiation. Sporadic chamber measurements are based on the assumption of a constant emission flux from the soil into the atmosphere. Thereby it is ignored that the pressure field, the stratification of the atmosphere and the turbulence can modify the emission rate, at least the emission at the top of the surface. But it is impossible to abstain from chamber measurements, because measurements in the atmosphere have a too large footprint for probing single plots. Furthermore, non-transparent chambers can measure the respiration at daytime too. To reduce errors under atmospheric conditions, the following measurement design is possible: Parallel measurements with eddy-covariance techniques on a nearby larger plot with a chamber in the maximum of the footprint for comparison.

One of the oldest chamber types and nearly 100 years in use is the non-flow-through steady-state chamber. These chambers are fully closed with an absorber inside. As an example, the respired carbon dioxide can be measured with an alkali absorber. After some hours or days, the absorber must be chemically analyzed. This type of chamber is however nowadays rarely used except for isotope labeling techniques. Non-steady-state chambers are now the most common. Thereby, in the case of emission from the soil, the concentration inside the chamber increases in a time interval of some minutes, while the concentration is continuously measured. From the slope of the concentration increase the emission can be calculated. To realize a linear slope the chamber must be ventilated or equipped with a pressure vent at the top of the chamber (Xu et al. 2006). Another system, the flow-through non-steady-state chamber, works with a constant air flow through the ventilated chamber, where the concentration is measured at the in- and out-flow. The benefit is a high time resolution of the measurements, but the gas analyzers

need a high accuracy and sampling frequency. Accordingly, these chambers are only available for some gases.

Due to the large number of chamber types and the relatively low number of commercially available chambers, chamber comparison studies were often conducted (Pumpanen et al. 2004; Pihlatie et al. 2013) and good agreement was generally observed. Also the comparison automatic chamber and eddy-covariance measurements compare well over longer time periods (Rochette et al. 1997; Wang et al. 2013; Riederer et al. 2014). However, single measurements often differ significantly due to various factors. The dependence on the degree of turbulence (friction velocity) shows good agreement for chambers when turbulence is low and underestimation for higher levels of turbulence (Lai et al. 2012). Obviously, in the range of a good agreement the ventilation of the chamber is similar to the conditions outside the chamber. The adjusted longwave net radiation inside the chamber is often very much underestimated, while outside large values are possible with cooling at the surface resulting in stable stratification. Under these conditions, during the night or during the oasis effect in the late afternoon, chambers overestimate the fluxes significantly. But in the case of coherent structures, which realize a well-mixed situation over a short period, even at night, smaller fluxes are measured in the chamber (Riederer et al. 2014). These complex findings corroborate the above given recommendation, to permanently measure at the same site with both eddy-covariance and chamber methods, such that corrections for single cases are possible.

6.2.6.3 Measurements at Plants

Even though measurements at plants are not the task of meteorologists, many plant parameters are used for modelling the energy and matter exchange (see Chap. 5). Since good textbooks are now available (Monteith and Unsworth 2008; Hari et al. 2013; Moene and van Dam 2014; Monson and Baldocchi 2014), only the most important parameters are described.

Probably the most important parameter is the leaf-area-index (*LAI*), which gives the contribution of the leaf surface per area element (see Table 5.11). It can be determined by spectral radiation measurements in the photosynthetic active range (*PAR)*. Thus, the radiation below leafs will be compared with the radiation without any influence of the biomass.

The leaf area index can be relatively easily determined with remote sensing methods. The satellite images must be corrected for atmospheric influences before application to ensure the comparability of different pictures. For evaluation of single pictures, such corrections are not needed (Song et al. 2001). For the determination of the *LAI* value the Normalized Difference Vegetation Index (*NDVI*) is applied, which is the difference of the spectral channels of the red light (0.63–0.69 μm) and the near infrared (0.76–0.90 μm):

$$NDVI = \frac{NIR - red}{NIR + red} \tag{6.50}$$

Often the vertical distribution of the leaf area density (*LAD*) is also necessary and sometimes even the available leaf mass is of interest, but for this determination a harvesting of leaves is necessary. Instead of the leaf area index the plant area index (*PAI*), which includes besides the leaves also the branches and the steam, can also be used. It must be taken into account that the dependence of the *LAI* and *NDVI* becomes saturated for *LAI* > 8–10 and in this range the *LAI* cannot be accurately determined from *NDVI* data.

While the *NDVI* has a strong sensitivity on chlorophyll, the Enhanced Vegetation Index (*EVI*) better represents the plant structure together with *LAI* (Huete et al. 2002). It can be determined by including the blue light (0.459–0.479 μm):

$$EVI = G \cdot \frac{NIR - red}{NIR + C1 \cdot red - C2 \cdot blue + L} \tag{6.51}$$

The amplification factor is $G = 2.5$, the other factors are $C1 = 6$, $C2 = 7.5$, and $L = 1$. If no spectral measurements of the blue band are available, the factors are $C1 = 2.4$ and $C2 = 0$.

6.2.6.4 *Direct Evaporation Measurement*

The determination of the evaporation is a very important task. Prior to micrometeorological studies various devices were developed, especially in agrometeorology such as the evaporimeter according to Piche with absorbent paper as evaporation area or the evaporation instrument according to Czeratzki with porous clay plates, all of which are no longer used (Hupfer and Kuttler 2006).

For evaporation measurements in agrometeorology lysimeters are applied, which are a good direct measurement technique if applied correctly. The benefit is that contrary to micrometeorological measurements, only small areas are necessary.

Especially in hydrological networks, evaporation pans are still used, mainly the Class-A-Pan (DeFelice 1998). It is a round pan with 1.14 m² water surface (diameter 120.65 cm, height 25.4 cm) and 15.2–17.8 cm water depth. The evaporation is measured by the water loss in the pan, and complicated corrections (Linacre 1994; Sentelhas and Folegatti 2003) based on wind velocity, atmospheric moisture, and water temperature must be made. A greatly simplified but reliable method for daily sums of the evaporation (Smajstrla et al. 2000) uses the height difference of the water level in the evaporation pan corrected with the precipitation

$$Q_E = Kp \left(h_{day \ before} - h_{measuring \ day} \right) \tag{6.52}$$

Table 6.15 Coefficient Kp for the determination of the evaporation with the Class-A-Pan according to Eq. (6.55) for meadows or grain (in brackets for bare soil) in the vicinity of the device (Doorenbos and Pruitt 1977; Smajstrla et al. 2000)

Mean wind velocity at the measurement date	Extension of the area in the surrounding in m	Minimum of the relative humidity at the measurement date	
		>40%	<40%
low ≤ 2 ms^{-1}	1	0.65 (0.80)	0.75 (0.85)
	10	0.75 (0.70)	0.85 (0.80)
	100	0.80 (0.65)	0.85 (0.75)
	1000	0.85 (0.60)	0.85 (0.70)
moderate 2.1–4.4 ms^{-1}	1	0.60 (0.75)	0.65 (0.80)
	10	0.70 (0.65)	0.75 (0.70)
	100	0.75 (0.60)	0.80 (0.65)
	1000	0.80 (0.55)	0.80 (0.60)
strong ≥ 4.5 ms^{-1}	1	0.50 (0.65)	0.60 (0.70)
	10	0.60 (0.55)	0.65 (0.65)
	100	0.65 (0.50)	0.70 (0.60)
	1000	0.70 (0.45)	0.75 (0.55)

(in mm d^{-1}). Correction factors, which are functions of wind velocity, minimum relative humidity, and the conditions in the surrounding environment of the pan are given in Table 6.15.

6.3   Quality Assurance

Measurements are now widely automated, and based on modern measurement and electronic data storage techniques. But it is a fallacy to believe this saves man-power, because uncontrolled measurement data are not very reliable or may be worthless. The expense of measurements has moved from manpower for obser-vation to manpower for quality assurance (QA), which requires measures that were formally covered by visual observations. Quality assurance includes several

important steps, which are partly interconnected (Shearman 1992; Smith et al. 1996; DeFelice 1998; VDI 2013).

6.3.1 Measurement Planning

During the planning of a measurement system, numerous questions must be taken into account. This starts with the data user giving clear instructions about the measurement resolutions in time and space, the requested representativeness, the accuracy, and the availability of the data, etc. This sounds easy, but it is often a big problem because users often have little knowledge of measurement methodology and technology, and unrealistic requirements can occur. An interdisciplinary and iterative planning is necessary before a specification of the parameters can be made. This includes the technical parameters of the sensors, the units of the whole data sampling, transmitting and storing of the data, and data transfer to the user.

After this, follows the choice of suitable sensors, measurement sites, and data systems. Often large differences in price exist for apparently similar sensors. Therefore, detailed knowledge of the sensor characteristics and their influence on the whole project is necessary. Often in brochures, important information is missing and cannot be found elsewhere, because many low cost instruments are insufficiently investigated. Sensor lifetime, maintenance expenditure, and application under expected or extreme weather conditions are the deciding factors for high-end instruments. Sometimes special sensors must be developed. The micrometeorological requirements for the measurement sites are often so great that compromises are necessary, such as the exclusion of wind sectors or nighttime conditions with stable stratification. This must be done in agreement with the user requirements. For expensive measurement programs, it is required to test the measurement sites with a pre-experiment.

The largest part of the costs in running an experiment is the necessity for calibration and maintenance. Therefore, the periods for calibration (every 6–12 month for most of the systems) and maintenance (from a few days to several weeks depending on the specific maintenance work) must be determined, as well as the type of maintenance without data loss. This needs partly also investigation into calibration systems. Consideration of work safety is an important issue. In this complex, necessary corrections must be included, not only based on the calibration but also on the weather conditions.

A very important point is the definition of quality control (QC). This includes a possible daily control (visual or partly automatic) so that data failure or other defects can be immediately found. Only controlled and marked data must be stored in the database or go to the end user. Appropriate possibilities are extensively discussed in Sect. 6.3.2.

Because the data quality depends not only on the state of the sensor but also on the meteorological constraints, a complex quality management is necessary. Accordingly, the data should be flagged regarding the data control, if the data have

the necessary quality for usage, or if it can only be used for orientation. Such a system for the eddy-covariance method is shown in Sect. 4.2.5.

Feedback from the data user on further qualification of the system should not be underestimated. It is definitely a duty of the user and the initiator of the measurement program to insure that the data fulfil the desired objectives regarding the type of measurements and their quality. This can require some improvements or even reductions of the expenditure.

Quality assurance is a work package, which should not be underestimated with respect to the scope of the experiment. An increased attention for the running of the system helps in all cases.

6.3.2   Quality Control

Quality control has extremely important considerations. These include the control of the observations applying different criteria, and the indication of the data quality depending on the sensor and the meteorological conditions. Finally, the measured value gets a quality stamp.

The quality control can be made in different steps. The first step is the exclusion of missing data and obviously false data especially based on an electronic plausibility. The second step is assurance that the measured values are in the range of the measurement devices and in the possible meteorological range, which can change with the season. The resolution of the measured signal and its dependence on the digitalization must be controlled for the further calculations.

The meteorological tests follow, where typically comparisons are made with other observations. Complicated meteorological measurements need test models, e.g. boundary layer models, which test the combinations of all measured parameters. As a result of the test, a decision is necessary about the use of a manual or an automatic data correction, and the further use of the data. The storage in the database follows with a sufficient flagging, and information about the controls made, and probably also a quality stamp. All necessary steps are shown in Fig. 6.21.

After the initial tests, which can be automated, special tests on single parameters must be done (Fiebrich and Crawford 2001). The simplest cases are plausibility tests, e.g. for wind velocity and wind direction as shown in Table 6.16.

Tests for radiation components, more heavily use checks based on other meteorological parameters (Gilgen et al. 1994), where at least the components of the longwave radiation cannot easily be visually evaluated. For the upwelling longwave radiation, the test is to see if the radiation is within a certain difference of the radiation according to Stefan-Boltzmann law with the body temperature of the sensor:

$$\sigma(T_G - 5K)^4 \le I \uparrow \le \sigma(T_G + 5K)^4 \tag{6.53}$$

For strong longwave upwelling radiation during the night or strong heating of a dry soil, the threshold value of 5 K must be increased. For the atmospheric

Fig. 6.21 Flow diagram of the quality control steps for measured data (adapted from VDI 2013, with kind permission of © VDI e.V. and Beuth-Verlag, Berlin, 2013, All rights reserved)
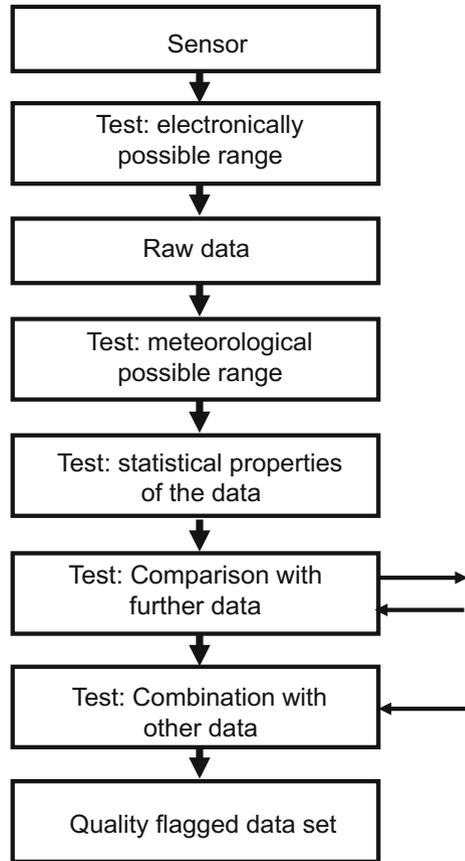
Table 6.16 Plausibility tests for wind velocity and direction (DeGaetano 1997)

Wind velocity	Wind direction
<0 ms^{-1}	
	<0° or >360°
<threshold velocity	for 1°–360°
>threshold velocity	for 0° (calm)
>60 ms^{-1} (height < 600 m a.s.l.)	

Measured values should be deleted if the data fall above or below the given thresholds

downwelling longwave radiation, the test is related to a black body (dome covered with water) and a grey body (clear sky with a radiation temperature of −55 °C):

$$0.7\,\sigma\,T_G^4 \leq I\uparrow\ \leq \sigma\,T_G^4 \tag{6.54}$$

For shortwave radiation the dependence on astronomical parameters and the transmission of the atmosphere is tested. For the reflected shortwave radiation the

test is made with the albedo (Table 1.1), where the albedo should only be calculated if the reflected radiation is >20–50 Wm^{-2}, otherwise large measurement errors occur. Values of the shortwave radiation at night, which differ from zero, should be set to zero and no offset correction should be applied.

Complicated micrometeorological measurements need a much higher quality control effort. For example, in the case of profile measurements comparisons with an approximation model can be used in the quality control and for assigning a quality criterion. Such comparisons can likely also provide information about possible internal boundary layers at the study site.

For many micrometeorological measurements, it is necessary to test if a fully turbulent regime is present. For eddy-covariance measurements, this can be done with a test on flux-variance similarities (Foken and Wichura 1996), as already shown in Sect. 4.2.5.

For large measurement programs, it is possible to compare different measurements. This can be in the simplest case the pure comparison of all wind and temperature data, where thresholds or altitude-dependent functions must be given. Also useful is the control of the energy balance, but the residual should be tested before selecting the measurement sites, the sensors, and the underlying surface. This should be taken into account by developing criteria (see Sect. 3.8), because the unclosed energy balance is specific for the measurement sites and not a quality criterion. Models, ranging from analytical up to meso-scale can be used for tests if the measured quantities are consistent with the model (Gandin 1988).

The quality control of meteorological measurements, especially of larger continuous measurement systems is still a developing question. Semi-automatic and fully automatic systems are only partly available. This is not only a question of software but also of research. Nevertheless, for available systems cases will be found where only experts are able to accurately separate meteorological effects from errors.

6.3.3   Intercomparison of Measurement Devices

Intercomparison experiments are an important requirement for the applications of sensors, because calibrations in wind tunnels and climate chambers have only a limited significance in the turbulent atmosphere. Such experiments also have high requirements on the terrain, which must be free of obstacles and allow an undisturbed installation of the sensors. The measurement heights should be chosen so that the near-surface gradients are small and do not have an influence on the measured results. The sensors for comparison should be in excellent condition and should have had a basic calibration.

Because in meteorology no absolute instruments exist for the comparisons, standards must be applied. These are devices, which were tested internationally over a long time and have shown constant results in previous comparisons. The sensor calibrations specification should be available.

For radiation measurements at the radiation centres, good standards are available. For turbulence measurements, this is a problem because wind tunnel calibrations of anemometers cannot simply be transferred to the turbulent flow. Nevertheless proven devices should be used, which have taken part in comparison experiments for at least 3–5 years.

The evaluations of comparisons are described with statistical numbers. One is the bias

$$b = \overline{(x_1 - x_2)} = \frac{1}{N} \sum_{i=1}^{N} (x_{1i} - x_{2i}), \qquad (6.55)$$

where subscript 1 is the device to be compared and subscript 2 the standard (etalon). The comparability gives the differences due to the device and the medium:

$$c = \left[\frac{1}{N} \sum_{i=1}^{N} (x_{1i} - x_{2i})^2 \right]^{1/2} \qquad (6.56)$$

The precision shows the systematic differences:

$$s = \left(c^2 - b^2 \right)^{1/2} \qquad (6.57)$$

If the measurement accuracy and the influences of the surrounding medium for both devices are nearly equal, a mean regression line can be calculated, which can also be used for correction purposes. Note, if there is no real independent device available and for correlation coefficients <0.99, than two regression lines must be calculated and averaged (Schönwiese 2013; VDI 2013). This is identical with the orthogonal regression (Supplement 6.3), which is the easiest case with a uniform distribution of the errors of both measured parameters; otherwise more complicated methods should be applied (Dunn 2004).

The results of in situ comparison experiments are not comparable with laboratory measurements because the stochastic character of atmospheric turbulence and many uncontrolled influencing factors always create scatter even for equal sensor types. In all comparisons, the standard deviation of the vertical wind component has the best results. In contrast, comparisons of fluxes are significantly poorer, and the largest scatter occurs for the friction velocity. Reasons for this are the different spectra of the vertical and horizontal wind velocity, especially with respect to the frequency of the maximum of energy.

Supplement 6.3 Orthogonal regression

For comparison of the measured signals of two sensors with i measurement points and approximately the same error (Dunn 2004), i.e. no one device is free of errors, the orthogonal regression can be applied. For the determination of the regression line

$$\bar{y} = a\bar{x} + b \tag{S6.5}$$

the correlation coefficient is set to 1.0. With the mean value

$$\bar{m} = \frac{1}{N} \sum_{i=1}^{N} m_i \tag{S6.6}$$

and the variance of the measured data

$$\sigma(m)^2 = \frac{1}{N-1} \sum_{i=1}^{N} (m_i - \bar{m})^2 \tag{S6.7}$$

follows for the slope of the regression line

$$a = \frac{\sigma(y)}{\sigma(x)} \tag{S6.8}$$

and by application of a in Eq. (S6.5) the systematic difference (intercept) can be determined.

References

Albrecht F (1927) Thermometer zur Messung der wahren Temperatur. Meteorol Z. 24:420–424.

Andreas EL (1989) Two-wavelength method of measuring path-averaged turbulent surface heat fluxes. J Atm Oceanic Techn. 6:280–292.

Assmann R (1887) Das Aspirationspsychrometer, ein neuer Apparat zur Ermittlung der wahren Temperatur und Feuchtigkeit der Luft. Das Wetter. 4:245–286.

Assmann R (1888) Das Aspirationspsychrometer, ein neuer Apparat zur Ermittlung der wahren Temperatur und Feuchtigkeit der Luft. Das Wetter. 5:1–22.

Bartels J (1935) Zur Morphologie geophysikalischer Zeitfunktionen. Sitzungsberichte Preuß Akad Wiss. 30:504–522.

Bentley JP (2005) Principles of Measurement Systems. Pearson Prentice Hall, Harlow 528 pp.

Beyrich F, DeBruin HAR, Meijninger WML, Schipper JW and Lohse H (2002) Results from one-year continuous operation of a large aperture scintillometer over a heterogeneous land surface. Boundary-Layer Meteorol. 105:85–97.

Bovscheverov VM and Voronov VP (1960) Akustitscheskii fljuger (Acoustic rotor). Izv AN SSSR, ser Geofiz. 6:882–885.

Bowen AJ and Teunissen HW (1986) Correction factors for the directional response of Gill propeller anemometer. Boundary-Layer Meteorol. 37:407–413.

Braud J, Noilhan P, Bessemoulin P, Mascart P, Haverkamp R and Vauclin M (1993) Bare ground surface heat and water exchanges under dry conditions. Boundary-Layer Meteorol. 66:173–200.

Brock FV and Richardson SJ (2001) Meteorological Measurement Systems. Oxford University Press, New York, 290 pp.

Buck AL (1973) Development of an improved Lyman-alpha hygrometer. Atm Technol. 2:213–240.

de Vries DA (1963) Thermal Properties of Soils. In: van Wijk WR (ed.), Physics of the Plant Environment. North-Holland Publ. Co., Amsterdam, 210–235.

DeBruin HAR (2002) Introduction: Renaissance of scintillometry. Boundary-Layer Meteorol. 105:1–4.

DeBruin HAR, Meijninger WML, Smedman A-S and Magnusson M (2002) Displaced-beam small aperture scintillometer test. part I: The WINTEX data-set. Boundary-Layer Meteorol. 105:129–148.

DeFelice TP (1998) An introduction to meteorological instrumentation and measurement. Prentice Hall, Upper Saddle River, 229 pp.

DeGaetano AT (1997) A quality-control routine for hourly wind observations. J Atm Oceanic Techn. 14:308–317.

Denmead OT (2008) Approaches to measuring fluxes of methane and nitrous oxide between landscapes and the atmosphere. Plant Soil. 309:5–24.

DIN-EN (2009) Industrial platinum resistance thermometers and platinum temperature sensors (Industrielle Platin-Widerstandsthermometer und Platin Sensoren), IEC 60751:2008. Beuth-Verlag, Berlin, DIN-EN 60751, 28 pp.

Doetsch G (1985) Anleitung zum praktischen Gebrauch der Laplace-Transformation und der Z-Transformation. Oldenbourg, München, Wien, 256 pp.

Doorenbos J and Pruitt WO (1977) Guidelines for predicting crop water requirements. FAO Irrigation Drainage Pap. 24, 2nd ed.:145 pp.

Drinkov R (1972) A solution to the paired Gill-anemometer response function. J Climate Appl Meteorol. 11:76–80.

Dunn G (2004) Statistical Evaluation of Measurement Errors. Arnold, London, 216 pp.

Edwards GC, Neumann HH, den Hartog G, Thurtell GW and Kidd G (1994) Eddy correlation measurements of methane fluxes using a tunable diode laser at the Kinosheo Lake tower site during the Northern Wetlands Study (NOWES). J Geophys Res. 99 D1:1511–1518.

Elagina LG (1962) Optitscheskij pribor dlja izmerenija turbulentnych pulsacii vlaschnosti (Optical sensor for the measurement of turbulent humidity fluctuations). Izv AN SSSR, ser Geofiz. 12:1100–1107.

Emeis S (2010) Measurement Methods in Atmospheric Sciences. Borntraeger Science Publishers, Stuttgart, 257 pp.

Fiebrich CA and Crawford KL (2001) The impact of unique meteorological phenomena detected by the Oklahoma Mesonet and ARS Micronet on automatic quality control. Bull Amer Meteorol Soc. 82:2173–2187.

Foken T (1979) Temperaturmessung mit dünnen Platindrähten. Z Meteorol. 29:299–307.

Foken T, Kaiser H and Rettig W (1983) Propelleranemometer: Überblick und spezielle Entwicklungen am Meteorologischen Hauptobservatorium Potsdam. Veröff Meteorol Dienstes DDR. 24:48 pp.

Foken T, Dlugi R and Kramm G (1995) On the determination of dry deposition and emission of gaseous compounds at the biosphere-atmosphere interface. Meteorol Z. 4:91–118.

Foken T and Oncley SP (1995) Results of the workshop 'Instrumental and methodical problems of land surface flux measurements'. Bull Amer Meteorol Soc. 76:1191–1193.

Foken T and Wichura B (1996) Tools for quality assessment of surface-based flux measurements. Agrical Forest Meteorol. 78:83–105.

Foken T, Buck AL, Nye RA and Horn RD (1998) A Lyman-alpha hygrometer with variable path length. J Atm Oceanic Techn. 15:211–214.

Foken T and Falke H (2012) Technical note: Calibration device for the krypton hygrometer KH20. Atmos. Meas. Tech. 5:1861–1867.

Frankenberger E (1951) Untersuchungen über den Vertikalaustausch in den unteren Dekametern der Atmosphäre. Ann Meteorol. 4:358–374.

Fuchs M (1986) Heat flux. In: Klute A (ed.), Methods of Soil Analysis, Part 1: Physical and Mineralogical Methods, 2nd edn., vol 9. ASA and SSSA, Madison, WI, 957–968.

Gandin LS (1988) Complex quality control of meteorological observations. Monthly Weather Review. 116:1137–1156.

Gilgen H, Whitlock CH, Koch F, Müller G, Ohmura A, Steiger D and Wheeler R (1994) Technical plan for BSRN data management. World Radiation Monitoring Centre (WRMC), Technical Report. 1:56 pp.

Graf U (2004) Applied Laplace transforms and z-transforms for scientists and engineers. Birkhäuser, Basel, 500 pp.

Halldin S and Lindroth A (1992) Errors in net radiometry, comparison and evaluation of six radiometer designs. J Atm Oceanic Techn. 9:762–783.

Hanafusa T, Fujitana T, Kobori Y and Mitsuta Y (1982) A new type sonic anemometer-thermometer for field operation. Papers Meteorol Geophys. 33:1–19.

Hari P, Heliövaara K and Kulmala L (eds) (2013) Physical and Physiological Forest Ecology. Springer, Dordrecht, Heidelberg, New York, London, 534 pp.

Harrison GR (2015) Meteorological Measurements and Instrumentations. John Wiley and Sons, Chichester, 257 pp.

Haugen DA (1978) Effects of sampling rates and averaging periods on meteorological measurements. Fourth Symp Meteorol Observ Instr, Am Meteorol Soc:15–18.

Hayden KL, Anlauf KG, Hoff RM, Strapp JW, Bottenheim JW, Wiebe HA, Froude FA, Martin JB, Steyn DG and McKendry IG (1997) The vertical chemical and meteorological structure of the boundary layer in the Lower Fraser Valley during Pacific '93. Atmos Environm. 31:2089–2105.

Hebra AJ (2010) The Physics of Metrology. Springer, Wien, New York 383 pp.

Helmis CG, Sgouros G, Tombrou M, Schäfer K, Münkel C, Bossioli E and Dandou A (2012) A comparative study and evaluation of mixing-height estimation based on sodar-RASS, ceilometer data and numerical model simulations. Boundary-Layer Meteorol. 145:507–526.

Hill MK and Clifford SF (1978) Modified spectrum of atmospheric temperature fluctuations and its application to optical propagation. J Opt Soc Am. 68:892–899.

Hill R (1997) Algorithms for obtaining atmospheric surface-layer from scintillation measurements. J Atm Oceanic Techn. 14:456–467.

Hill RJ, Clifford SF and Lawrence RS (1980) Refractive index and absorption fluctuations in the infrared caused by temperature, humidity and pressure fluctuations. J Opt Soc Am. 70:1192–1205.

Horton R, Wieringa PJ and Nielsen DR (1983) Evaluation of methods for determining the apparent thermal diffusivity of soil near the surface. Soil Sci Soc Am J. 47:25–32.

Hübner J, Olesch J, Falke H, Meixner FX and Foken T (2014) A horizontal mobile measuring system for atmospheric quantities. Atmos Meas Techn. 7:2967–2980.

Huete A, Didan K, Miura T, Rodriguez EP, Gao X and Ferreira LG (2002) Overview of the radiometric and biophysical performance of the MODIS vegetation indices. Rem Sens Environm. 83:195–213.

Hupfer P and Kuttler W (eds) (2006) Witterung und Klima, begründet von Ernst Heyer. B. G. Teubner, Stuttgart, Leipzig, 554 pp.

ISO (1990) Solar energy - Specification and classification of instruments for measuring hemispherical solar and direct solar radiation, ISO 9060. Beuth-Verlag, Berlin, 21 pp.

ISO (1996) Acoustics - Attenuation of sound during propagation outdoors - Part 2: General method of calculation, ISO 9613–2. Beuth-Verlag, Berlin, 26 pp.

ISO (2002) Meteorology -Sonic anemometer/thermometer - Acceptance test method for mean wind measurements, ISO 16622. Beuth-Verlag, Berlin, 21 pp.

ISO (2007) Meteorology - Wind measurements - Part 1: Wind tunnel test methods for rotating anemometer performance. ISO 17713–1. Beuth-Verlag, Berlin, 17 pp.

Jacobs AFG and McNaughton KG (1994) The excess temperature of a rigid fast-response thermometer and its effects on measured heat fluxes. J Atm Oceanic Techn. 11:680–686.

Junghans (1967) Der Einfluß es Windes auf das Niederschlagsdargebot von Hängen. Archiv Forstw. 16:579–585.

Kaimal JC and Businger JA (1963) A continuous wave sonic anemometer-thermometer. J Climate Appl Meteorol. 2:156–164.

Kaimal JC and Gaynor JE (1991) Another look to sonic thermometry. Boundary-Layer Meteorol. 56:401–410.

Kaimal JC and Finnigan JJ (1994) Atmospheric Boundary Layer Flows: Their Structure and Measurement. Oxford University Press, New York, NY, 289 pp.

Kallistratova MA (1959) Eksperimentalnoje issledovanie rassejenija zvuka v turbulentnoj atmosfere (An experimental investigation in the scattering of sound in the turbulent atmosphere). Dokl AN SSSR. 125:69–72.

Kasten F (1985) Maintenance, calibration and comparison. Instrum Obs Methods Rep. 23 (WMO/TD 51):65–84.

Kleinschmidt E (ed) (1935) Handbuch der meteorologischen Instrumente und ihrer Auswertung. Springer, Berlin, 733 pp.

Kretschmer SI (1954) Metodika izmerenija mikropulsacii skorosti vetra i temperatura v atmosfere (A method to measure the fluctuations of the wind velocity and the temperature). Trudy geofiz inst AN SSSR. 24 (151):43–111.

Kretschmer SI and Karpovitsch JV (1973) Maloinercionnyj ultrafioletovyj vlagometer (Sensitive ultraviolet hygrometer). Izv AN SSSR, Fiz Atm Okeana. 9:642–645.

Kristensen L (1998) Cup anemometer behavior in turbulent environments. J Atm Oceanic Techn. 15:5–17.

Lai DYF, Roulet NT, Humphreys ER, Moore TR and Dalva M (2012) The effect of atmospheric turbulence and chamber deployment period on autochamber CO_2 and CH_4 flux measurements in an ombrotrophic peatland. Biogeosci. 9:3305–3322.

Latimer JR (1972) Radiation measurement, International Field Year of the Great Lakes, Techn. Manual Series No. 2, Information. Ottawa, 53 pp.

Leuning R and Judd MJ (1996) The relative merits of open- and closed path analysers for measurements of eddy fluxes. Global Change Biology. 2:241–254.

Liebethal C, Huwe B and Foken T (2005) Sensitivity analysis for two ground heat flux calculation approaches. Agrical Forest Meteorol. 132:253–262.

Liebethal C and Foken T (2006) On the use of two repeatedly heated sensors in the determination of physical soil parameters. Meteorol Z. 15:293–299.

Liebethal C and Foken T (2007) Evaluation of six parameterization approaches for the ground heat flux. Theor Appl Climat. 88:43–56.

Linacre ET (1994) Estimating U.S. Class-A pan evaporation from climate data. Water Internat. 19:5–14.

Martini L, Stark B and Hunsalz G (1973) Elektronisches Lyman-Alpha-Feuchtigkeitsmessgerät. Z Meteorol. 23:313–322.

Mauder M, Liebethal C, Göckede M, Leps J-P, Beyrich F and Foken T (2006) Processing and quality control of flux data during LITFASS-2003. Boundary-Layer Meteorol. 121:67–88.

Mayer J-C, Hens K, Rummel U, Meixner FX and Foken T (2009) Moving measurement platforms —specific challenges and corrections. Meteorol Z. 18:477–488.

McAllister LG, Pollard JR, Mahoney AR and Shaw PJR (1969) Acoustic sounding - A new approach to the study of atmospheric structure. Proc IEEE. 57:579–587.

Meijninger WML, Green AE, Hartogensis OK, Kohsiek W, Hoedjes JCB, Zuurbier RM and DeBruin HAR (2002) Determination of area-averaged water vapour fluxes with large aperture and radio wave scintillometers over a heterogeneous surface - Flevoland Field Experiment. Boundary-Layer Meteorol. 105:63–83.

Meijninger WML, Lüdi A, Beyrich F, Kohsiek W and DeBruin HAR (2006) Scintillometer-based turbulent surface fluxes of sensible and latent heat over heterogeneous a land surface - A contribution to LITFASS-2003. Boundary-Layer Meteorol. 121:89–110.

Mitsuta Y (1966) Sonic anemometer-thermometer for general use. J Meteor Soc Japan. Ser. II, 44:12–24.

Moene AF and van Dam JC (2014) Transport in the Atmosphere-Vegetation-Soil Continuum. Cambridge University Press, Cambridge, 436 pp.

Moncrieff JB, Massheder JM, DeBruin H, Elbers J, Friborg T, Heusinkveld B, Kabat P, Scott S, Søgaard H and Verhoef A (1997) A system to measure surface fluxes of momentum, sensible heat, water vapor and carbon dioxide. J Hydrol. 188–189:589-611.

Monson R and Baldocchi D (2014) Terrestrial Biosphere-Atmosphere Fluxes. Cambridge University Press, New York, XXI, 487 pp.

Monteith JL and Unsworth MH (2008) Principles of Environmental Physics, 3rd edition. Elsevier, Academic Press, Amsterdam, Boston, 418 pp.

Moore CJ (1986) Frequency response corrections for eddy correlation systems. Boundary-Layer Meteorol. 37:17–35.

Münkel C, Eresmaa N, Räsänen J and Karppinen A (2007) Retrieval of mixing height and dust concentration with lidar ceilometer. Boundary-Layer Meteorol. 124:117–128.

Neff WD and Coulter RL (1986) Acoustic remote sounding. In: Lenschow DH (ed.), Probing the Atmospheric Boundary Layer. American Meteorological Society, Boston, 201–236.

Ohmura A, Dutton EG, Forgan B, Fröhlich C, Gilgen H, Hegner H, Heimo A, König-Langlo G, McArthur B, Müller G, Philipona R, Pinker R, Whitlock CH, Dehne K and Wild M (1998) Baseline Surface Radiation Network (BSRN/WCRP): New precision radiometry for climate research. Bull Amer Meteorol Soc. 79:2115–2136.

Orlanski I (1975) A rational subdivision of scales for atmospheric processes. Bull. Am. Meteorol. Soc. 56:527–530.

Pattey E, Strachan IB, Desjardins RL, Edwards GC, Dow D and MacPherson IJ (2006) Application of a tunable diode laser to the measurement of CH_4 and N_2O fluxes from field to landscape scale using several micrometeorological techniques. Agrical Forest Meteorol. 136:222–236.

Philip JR (1961) The theory of heat flux meters. J Geophys Res. 66:571–579.

Philipona R, Fröhlich C and Betz C (1995) Characterization of pyrgeometers and the accuracy of atmospheric long-wave radiation measurements. Applied Optics. 34:1598–1605.

Philipona R, Dutton EG, Stoffel T, Michalsky J, Reda I, Stifter A, Wendung P, Wood N, Clough SA, Mlawer EJ, Anderson G, Revercomb HE and Shippert TR (2001) Atmospheric longwave irradiance uncertainty: Pyrgeometers compared to an absolute sky-scanning radiometer, atmospheric emitted radiance interferometer, and radiative transfer model calculations. J Geophys Res: Atmosph. 106:28129–28141.

Pihlatie MK, Christiansen JR, Aaltonen H, Korhonen JFJ, Nordbo A, Rasilo T, Benanti G, Giebels M, Helmy M, Sheehy J, Jones S, Juszczak R, Klefoth R, Lobo-do-Vale R, Rosa AP, Schreiber P, Serça D, Vicca S, Wolf B and Pumpanen J (2013) Comparison of static chambers to measure CH_4 emissions from soils. Agrical Forest Meteorol. 171–172:124–136.

Profos P and Pfeifer T (eds) (1997) Grundlagen der Meßtechnik. Oldenbourg, München, Wien, XIII, 367 pp.

Pumpanen J, Kolari P, Ilvesniemi H, Minkkinen K, Vesala T, Niinistö S, Lohila A, Larmola T, Morero M, Pihlatie M, Janssens I, Yuste JC, Grünzweig JM, Reth S, Subke J-A, Savage K, Kutsch W, Østreng G, Ziegler W, Anthoni P, Lindroth A and Hari P (2004) Comparison of different chamber techniques for measuring soil CO2 efflux. Agrical Forest Meteorol. 123:159–176.

Richardson SJ, Brock FV, Semmer SR and Jirak C (1999) Minimizing errors associated with multiplate radiation shields. J Atm Oceanic Techn. 16:1862–1872.

Richter D (1995) Ergebnisse methodischer Untersuchungen zur Korrektur des systematischen Meßfehlers des Hellmann-Niederschlagsmessers. Ber. d. Dt. Wetterdienstes. 194:93 pp.

Riederer M, Serafimovich A and Foken T (2014) Eddy covariance—chamber flux differences and its dependence on atmospheric conditions. Atmospheric Measurement Techniques. 7:1057–1064.

Rink J (1961) Thermistore und ihre Anwendung in der Meteorologie. Abh Meteorol Hydrol Dienstes DDR. 63:58 pp.

Rochette P, Ellert B, Gregorich EG, Desjardins RL, Pattey E, Lessard R and Johnson BG (1997) Description of a dynamic closed chamber for measuring soil respiration and its comparison with other techniques. Can J Soil Sci. 77:195–203.

Rochette P and Hutchinson GL (2005) Measurement ofsoil respiration in situ: Chamber techniques. In: Hatfield JL and Baker I (eds.), Micrometeorology in Agricultural Systems, vol 47. American Society of Agronomy, Madison, 247–286.

Sauer TJ, Harris AR, Ochsner TE and Horton R (2002) Errors in soil heat flux measurement: Effects of flux plate design and varying soil thermal properties. 25th Symp Agric & Forest Meteor:11–12.

Schönwiese C-D (2013) Praktische Statistik für Meteorologen und Geowissenschaftler. Borntraeger, Stuttgart, 319 pp.

Schrüfer E, Reindl L and Zagar B (2014) Elektrische Messtechnik. Fachbuchverlag im Carl Hanser Verlag, Leipzig, München, 445 pp.

Sentelhas PC and Folegatti MV (2003) Class A pan coefficients (Kp) to estimate daily reference evapotranspiration (ETo). Revista Brasilleira de Engenharia Agricola e Ambiental. 7:111–115.

Sevruk B (1981) Methodische Untersuchungen des systematischen Messfehlers der Hellmann-Regenmesser im Sommerhalbjahr in der Schweiz. Mitt. d. Versuchsanstalt f. Wasserb., Hydrol. u. Glaziol. 52:290 pp.

Shearman RJ (1992) Quality assurance in the observation area of the Meteorological Office. Meteorol Mag. 121:212–216.

Smajstrla AG, Zazueta FS, Clark GA and Pitts DJ (2000) Irrigation scheduling with evaporation pans. Univ of Florida, IFAS Ext Bul 254,9 pp.

Smith SR, Camp JP and Legler DM (1996) Handbook of Quality Control, Procedures and Methods for Surface Meteorology Data. Center for Ocean Atmospheric Prediction Studies, TOGA/COARE, Technical Report. 96–3:60 pp. [Available from Florida State University, Tallahassee, FL, 32306-33041].

Song C, Woodcock CE, Seto KC, Lenney MP and MacOmber SA (2001) Classification and change detection using Landsat TM data: when and how to correct atmospheric effects? Rem Sens Environm. 75:230–244.

Sonntag D (1966–1968) Hygrometrie. Akademie-Verlag, Berlin, 1086 pp.

Sonntag D, Scholz K and Schulze K (1989) The psychrometer equation for Assmann aspiration psychrometer for use in meteorological practice. Instrum Obs Methods Rep. 35 (WMO/TD No. 303):175–180.

Sonntag D (1994) Advancements in the field of hygrometry. Meteorol Z. 3:51–66.

Sturm P, Eugster W and Knohl A (2012) Eddy covariance measurements of CO_2 isotopologues with a quantum cascade laser absorption spectrometer. Agrical Forest Meteorol. 152:73–82.

Tatarski VI (1961) Wave Propagation in a Turbulent Medium. McGraw-Hill, New York, 285 pp.

Taubenheim J (1969) Statistische Auswertung geophysikalischer und meteorologischer Daten. Geest & Portig, Leipzig, 386 pp.

Thiermann V and Grassl H (1992) The measurement of turbulent surface layer fluxes by use of bichromatic scintillation. Boundary-Layer Meteorol. 58:367–391.

Tsvang LR (1960) Izmerenija tschastotnych spektrov temperaturnych pulsacij v prizemnom sloe atmosfery (Measurement of the spectra of the temperature fluctuations in the near surface layer of the atmosphere). Izv AN SSSR, ser Geofiz. 10:1252–1262.

van der Hegge Zijnen BG (1956) Modified correlation formulae for heat transfer by natural and by forced convection from horizontal cylinders. Appl Sci Res. A6:129–140.

van Loon WKP, Bastings HMH and Moors EJ (1998) Calibration of soil heat flux sensors. Agrical Forest Meteorol. 92:1–8.

VDI (2000) Umweltmeteorologie, Meteorologische Messungen für Fragen der Luftreinhaltung - Wind, VDI 3786 Blatt2. Beuth-Verlag, Berlin, VDI 3786, Blatt 2, 33 pp.

VDI (2006) Umweltmeteorologie - Meteorologische Messungen - Messstation, VDI 3786, Blatt 13. Beuth-Verlag, Berlin, 44 pp.

VDI (2013) Umweltmeteorologie - Meteorologische Messungen - Grundlagen (Environmental meteorology - Meteorological measurements - Basics), VDI 3786, Blatt 1. Beuth-Verlag, Berlin, 43 pp.

von Driest ER (1959) Convective heat transfer in gases. In: Lin CC (ed.), High speed aerodynamics and jet propulsion, Vol. V, Turbulent flow and heat transfer. Princeton University Press, Princeton, 339–427.

Vuerich E, Monesi C, Lanza LG, Stagi L and Lanzinger E (2009) WMO field intercomparison of rainfall intensity gauches. Instrum Obs Methods Rep. 99:1–290.

Wang K, Liu C, Zheng X, Pihlatie M, Li B, Haapanala S, Vesala T, Liu H, Wang Y, Liu G and Hu F (2013) Comparison between eddy covariance and automatic chamber techniques for measuring net ecosystem exchange of carbon dioxide in cotton and wheat fields. Biogeosci. 10:6865–6877.

Weitkamp C (2005) Lidar, Range-Resolved Optical Remote Sensing of the Atmosphere. Springer, New York, 456 pp.

Werle P, D'Amato F and Viciani S (2008) Tunable diode-laser spectroscopy: principles, performance, perspectives. In: Lackner M (ed.), Lasers in Chemistry - Probing Matter. Wiley-VCH, Weinheim, 255–275.

WMO (2008) Guide to meteorological instruments and methods of observation (updated 2010, 2012). WMO, Note. 8:7th edition.

Wyngaard JC and Clifford SF (1978) Estimating Momentum, Heat and Moisture Fluxes from Structure Parameters. J Atmos Sci. 35:1204–1211.

Xu L, Furtaw MD, Madsen RA, Garcia RL, Anderson DJ and McDermitt DK (2006) On maintaining pressure equilibrium between a soil CO2 flux chamber and the ambient air. J Geophys Res: Atmosph. 111:D08S10.